- Journals & Books
- Help
- Search

My account

Colorado School of Mines

- View **PDF**
- Download full issue

Outline

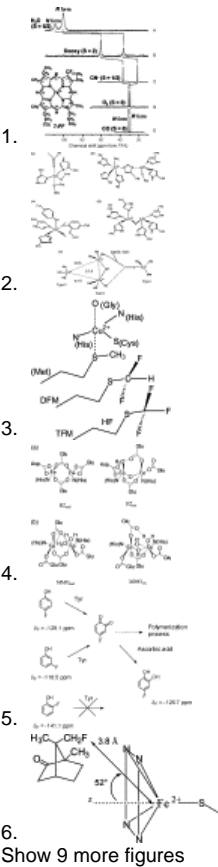## Cited by (18)

Figures (15)

1.

2.

3.

4.

5.

6.

Show 9 more figures

Tables (2)
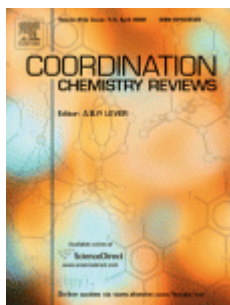
Review

^{19}F NMR: An underused efficient probe for paramagnetic metal centers in bioinorganic solution chemistry

Dedicated to Professor Jan Reedijk on the occasion of his 65th birthday.

Author links open overlay panelCatherine Belle, Claude Béguin, Sylvain Hamman, Jean-Louis Pierre

Show more

Add to Mendeley

Share

Cite

Abstract

The application of solution studies in bioinorganic chemistry through paramagnetic ^{19}F NMR is briefly reviewed. In Section 2 we summarize some theoretical aspects. Selected applications from bioinorganic chemistry (enzymes and models) can be found in Sections 3 and 4.

- Previous article in issue
- Next article in issue

Keywords

Metalloproteins

Biomimetic model complexes

^{19}F NMR

Paramagnetic metal centers

1. Introduction

As paramagnetic metal centers play a paramount role in the chemistry of metalloproteins and their biomimetic models, as well as simple transition metal complexes, specific tools for solution studies of their structure and their catalytic activities are requested.

Among the various spectroscopies used for these purposes, ^{19}F NMR seems to have been underused despite its great potentiality. The utility of ^{19}F NMR spectroscopy in biological molecules studies, in particular to probe protein structure has previously been demonstrated and was reviewed several years ago [1], [2], [3]. Fluorine NMR has also been applied to the study of biochemical mechanisms, metabolism, biodistribution, screening and pharmacokinetics of several fluorinated drugs.

In this manuscript the broad range of potential applicability of paramagnetic ^{19}F NMR in bioinorganic chemistry field (proteins and models) is reviewed with emphasis on selected examples, most of them from our work. Our goal is to bring forward an underused tool and impulse future utilization.

2. Methods

2.1. ^{19}F NMR: a brief reminder

^{19}F is a 100% naturally abundant nucleus with a nuclear spin I = 1/2. ^{19}F has a high-magnetogyric ratio γ, about 0.94 times that of ^{1}H (the reduced magnetogyric ratio γ_F value is 40.054 MHz T^{-1}). Therefore, its sensitivity, at constant field for equal number of nuclei, is 0.83 as compared to ^{1}H so that fluorine-containing compounds produce NMR signals that are nearly as easily detected as those of ^{1}H. For diamagnetic molecules, the range of chemical shifts for ^{19}F compounds is 20 or more times that of ^{1}H. For instance, the substituent effect in *para* substituted fluorobenzenes is about 20 ppm with the usual substituents (from p-NO$_2$ to p-OCH$_3$). This large effect provides a better resolution of signals and also a larger dynamic range giving an ability to differentiate between signals arising from species, which are in a dynamic equilibrium. ^{19}F chemical shifts are officially (IUPAC) reported with reference to external CFCl$_3$ [4]. Secondary references are ordinarily used as external C$_6$F$_6$ according to δ_F(C$_6$F$_6$) = –163 ppm relative to CFCl$_3$ or as external CF$_3$COOH according δ_F(CF$_3$COOH) = –79 ppm relative to CFCl$_3$. With the nuclear spin quantum 1/2, the relaxation is usually sufficiently long so that spin–spin splitting may be resolved easily.

Fluorine is particularly useful as a tracer in biological systems since there is essentially no natural background and the ^{19}F NMR signals are only related to the few ^{19}F nuclei in the ligand or in the protein. This labeling is particularly valuable from two points of view: (i) the Van der Waals radius of a fluorine atom is only slightly larger than that of an hydrogen atom, *i.e.* 135 and 110 pm for fluorine and hydrogen, respectively; (ii) at least when one fluorine is introduced in aromatic structures, there is a compensation of electronic effects giving only a small perturbation in the electronic structure of the molecule. Introduction of a strongly electron-withdrawing CF$_3$ or C$_6$F$_5$ group can induce marked effects on the physicochemical properties of the considered compound, however care should be taken regarding perturbations in the electronic structure of the molecule.

2.2. ^{19}F NMR and paramagnetism

The fluorine nucleus in paramagnetic metal systems as in molecular complexes or in metalloproteins is sensitive to the paramagnetic effect through the relaxation and the chemical shift parameters [5], [6], [7]. The effects can be considerable on relaxation, on chemical shift parameters or on both.

2.2.1. Electron-induced nuclear relaxation

The nuclear spin relaxation in a paramagnetic complex is induced by the electron–nucleus hyperfine interaction between the ^{19}F nucleus spin I and the electron spin S. This effect is characterized by the relaxation rate R_{iM} (1/T_{iM} where T_{iM} is the relaxation time) with i = 1 or 2 according to the spin–lattice or spin–spin mechanism of relaxation, respectively. The general effect is an enhancement and is commonly called paramagnetic relaxation enhancement (PRE). The set of equations for the relaxation rates in these systems are known [8], [9], [10], [11], [12], [13] as the Solomon–Bloembergen–Morgan (SBM) Eqs. (8), (9). These equations necessitate some comments before their detailed explanation.

The electron–nuclear hyperfine interaction between the nuclear spin (here the ^{19}F nucleus) and the electron spin consists mainly of two contributions:

(i)

The first term, the dipole–dipole (DD or dipolar) contribution or pseudo-contact coupling, results from the through-space dipolar interaction between the nuclear spin I and the electronic spin S. The derivation comes from the dipolar interaction Hamiltonian with the dipole–dipole coupling constant C_{DD} (in rad s^{-1}):

$$(1) \quad C_{DD} = \frac{\mu_0}{4\pi}\frac{\gamma_I \gamma_S}{r_{IS}^3}$$

with $\gamma_S\hbar = -g_S\mu_B$ and the other symbols having their usual meaning. This formula shows the decay of this constant with r_{IS}^{-3} (where r_{IS} is the electron–nucleus distance). The treatment needs the spectral density function of the intramolecular dipolar interaction. For an isotropic Brownian rotation of the complex, the corresponding auto-correlation function is monoexponential with one rotational correlation time τ_R, and its Fourier transform is a Lorentzian spectral density function depending on the angular frequency ω as

$$(2) \quad J(\omega, \tau_R) = \frac{\tau_R}{1 + \omega^2\tau_R^2}$$

The standard relaxation theory gives the following expressions for the longitudinal R_{1DD} and transversal R_{2DD} relaxation rate:

$$(3) \quad R_{1DD} = \frac{2}{15}C_{DD}^2 S(S+1)[J(\omega_S - \omega_I) + 3J(\omega_I) + 6J(\omega_S + \omega_I)]$$

$$(4) \quad R_{2DD} = \frac{1}{15}C_{DD}^2 S(S+1)[4J(0) + 3J(\omega_I) + J(\omega_S - \omega_I) + 6J(\omega_S) + 6J(\omega_S + \omega_I)]$$

As ω_I is much smaller than ω_S, the reduced formula gives

$$(5) \quad R_{1DD} \approx \frac{2}{15}C_{DD}^2 S(S+1)[3J(\omega_I) + 7J(\omega_S)]$$

$$(6) \quad R_{2DD} \approx \frac{1}{15}C_{DD}^2 S(S+1)[4J(0) + 3J(\omega_I) + 13J(\omega_S)]$$

The appropriate correlation times in the expression of the spectral density function are related to the fluctuations rate of the electron spin dipolar field caused by three main random motions:

(1)

The overall rotation of the complex characterized by the correlation time τ_R of the complex.

(2)

The chemical exchange rate of the metal bound ligand in dynamic equilibrium with the free ligand in the solution, characterized by the coordination lifetime τ_M. In most cases, we have $\tau_M \gg \tau_R$ and both are larger than the electronic relaxation time. Otherwise, the time correlation between the values of the interspin vector $\vec{r}_{IS}$ when the ligand changes from its bound to free states should be taken into account and the theory becomes significantly more complicated [14].

(3)

The rate of the statistical changes of the quantum states of the electronic spin characterized by the electronic relaxation rates of the R_{iS} of the complexed metal. The terms at frequencies 0 and ω_I correspond to the part of the dipolar Hamiltonian involving the component S_z of S, whereas the terms at frequencies $\omega_S - \omega_I$, and $\omega_S + \omega_I$, or simply ω_S, stem from the components S_+ or S_- of this Hamiltonian. The component S_z gives rise to the longitudinal relaxation rate R_{1S} and the components S_+ or S_- are at the origin of the transversal relaxation rate R_{2S}.

Therefore, the appropriate correlation times for the dipolar interaction are

$$(7) \quad \tau_{ci}^{-1} = \tau_R^{-1} + \tau_M^{-1} + R_{iS} \approx \tau_R^{-1} + R_{iS}$$

When one of these times is much shorter than the others, it effectively dominates τ_c. With some metal ions, R_{iS} dominates; but it is not the case for the metal ions considered in this review (Cu^{II}, Fe^{III}, Mn^{II}, Gd^{III}, …).

Finally, the formulas generally used to calculate the paramagnetic relaxation enhancements due to the electron–nuclear dipole–dipole coupling are

$$(8)\quad R_{1DD}\approx\frac{2}{15}C_{DD}^2 S(S+1)\left[\frac{3\tau_{c1}}{1+\omega_I^2\tau_{c1}^2}+\frac{7\tau_{c2}}{1+\omega_S^2\tau_{c2}^2}\right]$$

$$(9)\quad R_{2DD}\approx\frac{1}{15}C_{DD}^2 S(S+1)\left[4\tau_{c1}+\frac{3\tau_{c1}}{1+\omega_I^2\tau_{c1}^2}+\frac{13\tau_{c2}}{1+\omega_S^2\tau_{c2}^2}\right]$$

Recently, the theory of the PRE of nuclear spins as a function of magnetic field was thoroughly revisited [15], [16]. For the low-field cases (ω_I ■ the zero field splitting in the complex), the previous formulas should be unfortunately replaced by non-analytical equations. For the high-field cases (ω_I ■ ZFS), the last term of each formula have to be dropped and the high-field PRE can be approximated by the analytical expressions:

$$(10)\quad R_{1DD}^{high field}\approx\frac{2}{5}C_{DD}^2 S(S+1)\frac{\tau_{c1}}{1+\omega_I^2\tau_{c1}^2}$$

$$(11)\quad R_{2DD}^{high field}\approx\frac{1}{15}C_{DD}^2 S(S+1)\left[4\tau_{c1}+\frac{3\tau_{c1}}{1+\omega_I^2\tau_{c1}^2}\right]$$

(ii)

The second term is the through-bonds scalar coupling (SC) or Fermi contact coupling or hyperfine contribution. It arises from bond interactions between the fluorine nuclear spin and the spin of electron density at the site of observed nucleus. Its value is directly proportional to the local spin density in s-type atomic orbitals and allows derivation of the corresponding hyperfine coupling constant. This contact term is unaffected by the reorientation of the complex τ_R.

Starting from the Fermi contact interaction AIS, where I and S are the dimensionless spin operators for the fluorine nucleus and the paramagnetic electrons and A is the coupling constant (in rad s^{-1}), and introducing the appropriate spectral density function J_F, the Fermi contact contributions to the relaxation rates are [7], [9], [13]

$$(12)\quad R_{1SC}=\frac{2}{3}(A/\hbar)^2 S(S+1)J(\omega_S-\omega_I)\approx\frac{2}{3}(A/\hbar)^2 S(S+1)J(\omega_S)$$

$$(13)\quad R_{2SC}=\frac{1}{3}(A/\hbar)^2 S(S+1)[J(0)+J(\omega_S-\omega_I)]\approx\frac{1}{3}(A/\hbar)^2 S(S+1)[J(0)+J(\omega_S)]$$

The final standard Fermi contact formulas are

$$(14)\quad R_{1SC}=\frac{2}{3}(A/\hbar)^2 S(S+1)\frac{\tau'_{c2}}{1+\omega_S^2\tau'^2_{c2}}$$

$$(15)\quad R_{2SC}=\frac{1}{3}(A/\hbar)^2 S(S+1)\left[\tau'_{c1}+\frac{\tau'_{c2}}{1+\omega_S^2\tau'^2_{c2}}\right]$$

where τ'_{ci} is the appropriate correlation time for the Fermi contact relaxation. It differs from the previous τ_c correlation time for the dipole–dipole interaction, as the overall reorientation of the complex in solution has no effect on the contact term, *i.e.*

$$(16)\quad \tau'^{-1}_{ci}=\tau_M^{-1}+R_{iS}$$

Again, the simple Eqs. (14), (15) have to be replaced by non-analytical equations at low field [15], [16], whereas at high field, the contribution in ω_S has to be dropped.

(iii)

In deriving the dipolar and contact relaxation contributions due to the presence of unpaired electrons, the small difference in the population of the electron spin levels according to the Boltzmann distribution has been neglected. When this effect is taking into account, a time-averaged magnetic moment of the complex occurs and its interaction with the nuclear spins provides a further relaxation contribution, called magnetic susceptibility relaxation or Curie spin relaxation [7]. The corresponding correlation time is only determined by τ_R and τ_M according to

$$(17)\quad \tau''^{-1}_c=\tau_r^{-1}+\tau_M^{-1}\approx\tau_r^{-1}$$

The dipolar contributions to the relaxation rates provided by this mechanism are

$$(18)\quad R_{1DD}^{Curie}=\frac{2}{5}C_{DD}^2\left(\frac{B_0 g_S \mu_B S(S+1)}{3kT}\right)^2\frac{3\tau''_{c1}}{1+\omega_I^2\tau''^2_{c2}}$$

$$(19)\quad R_{2DD}^{Curie}=\frac{1}{5}C_{DD}^2\left(\frac{B_0 g_S \mu_B S(S+1)}{3kT}\right)^2\left(4\tau''_c+\frac{3\tau''_{c1}}{1+\omega_I^2\tau''^2_{c2}}\right)$$

(iv)

As ^{19}F nucleus is sensitive to the chemical shift anisotropy, the CSA mechanism could be present [7], [17]. As most of the studies are made at frequencies less than 500 MHz, this CSA effect is always shown to be negligible in comparison with the PRE.

2.2.2. Electron-induced paramagnetic chemical shift

The paramagnetic chemical shift (called also hyperfine shift or paramagnetic isotropic shift) $\Delta\delta_M$ can be defined as the difference $\Delta\delta_M = \delta_{obs} - \delta_D$, where δ_{obs} is the shift observed in the paramagnetic solution and δ_D is the diamagnetic chemical shift, which would be observed if the paramagnetic ion was replaced by a diamagnetic analog (*e.g.* Eu^{III}/Lu^{III} or Cu^{II}/Zn^{II}). This paramagnetic shift has two components, the pseudo-contact (or dipolar) contribution $\Delta\delta_{MDD}$ and the contact (or Fermi) contribution $\Delta\delta_{MSC}$:

(i)

The pseudo-contact contribution originates from the anisotropy of the paramagnetic susceptibility tensor of the complex. In the metal-centered point-dipole approximation, evaluation of the effect can be done, using the Cartesian components of the susceptibility tensor with the Cartesian axes chosen along the principal directions of this tensor, the classical expression for $\Delta\delta_{MDD}$ is [7], [18]

$$(20)\quad \Delta\delta_{MDD}=D_1(1-3\cos^2\theta)+D_2\sin^2\theta\cos2\phi$$

$$(21)\quad \text{with } D_1=\frac{1}{12\pi r_{IS}^3}\left[\chi_{zz}-\frac{1}{2}(\chi_{xx}+\chi_{yy})\right] \text{ and } D_2=\frac{1}{8\pi r_{IS}^3}(\chi_{xx}-\chi_{yy}),$$

respectively and r_{IS}, θ and ϕ are the polar coordinates of the interspin vector $\vec{r}_{IS}$ joining the nucleus under examination and the electronic spin in the principal axes system of the susceptibility tensor.

In the case of axial symmetry of the complex ($\chi_{xx} = \chi_{yy}$), the equation reduces to

$$(22)\quad \Delta\delta_{MDD}=D\frac{3\cos^2\theta-1}{r^3}$$

giving a zero pseudo-contact shift for $\theta = 54°44'$.

For a complex with only one thermally populated multiplet with spin S, the susceptibility terms χ_{ii} are related to the corresponding component g_{ii} of the tensor **g** according the following formula:

$$(23)\quad \chi_{ii}=\frac{N\mu_B^2 S(S+1)}{3k_B T}g_{ii}^2$$

The $\Delta\delta_{MDD}$ paramagnetic shift is therefore varying as T^{-1}.

In the presence of crystal field or zero-field splitting (ZFS) effects, the susceptibility tensor can be calculated through the Van Vleck equation [7], [18]. In general, these effects lead to an additional contribution in T^{-2} to $\Delta\delta_{MDD}$ [7], [19]. For ions of the first transition series, it can be shown that for axial symmetry with not too high values of $g_{||}^2-g_{\perp}^2$, the term in T^{-1} is small, but the term in T^{-2} is sizable [7], [20]. For paramagnetic Ln^{III} ions, but Gd^{III}, the term in T^{-2} is dominant [18], [19], [21].

(ii)

The contact shift is given by the magnetic field generated at the nucleus by the electron magnetic moment located at the nucleus itself, in relation with the spin density at the nucleus. This effect is therefore proportional to the contact coupling constant A, according to [7], [19]

$$(24) \quad \Delta\delta_{MSC} = A\blacksquare \frac{g S \mu_B S(S+1)}{3\gamma I k T}$$

The observed paramagnetic shift is the sum of the DD and SC contribution:

$$(25) \quad \Delta\delta_M = \Delta\delta_{MDD} + \Delta\delta_{MSC}$$

Finally, note that the theory presented here only applies to situations where the nuclear and electronic spins are located on the same molecule. When these spins are on two different species, theories of intermolecular paramagnetic relaxation enhancement and shift have to be used, the solvent being approximated either as a viscous continuum [7] or as an ensemble of discrete molecules [22], [23].

3. Applications to metalloproteins

The necessary requirement to obtain valuable information from ^{19}F NMR signals is to introduce an exogen fluorine atom. In metalloproteins several strategies have been used and are described below.

3.1. [19]F labeling heme and reconstitution of hemoproteins

This group of protein possesses unique physicochemical properties arising primarily from the presence of a heme group in the active center. Fluorinated heme syntheses associated with the reconstitution technique have been developed to introduce fluorine atom(s) into the active site of the proteins. Removal of the heme from the native protein leads to the apoprotein, which is reconstituted with a fluorinated heme. The ^{19}F NMR to study hemoproteins has received an intense interest for many years [24], [25]. A recent review by Yamamoto described in detail the applicability of ^{19}F NMR in b-type hemoproteins [26]. A large range of fluorine chemical shifts occur (described below; Fig. 1), corresponding to different oxidation, spin and ligation states as well as heme orientation, with respect of the protein.
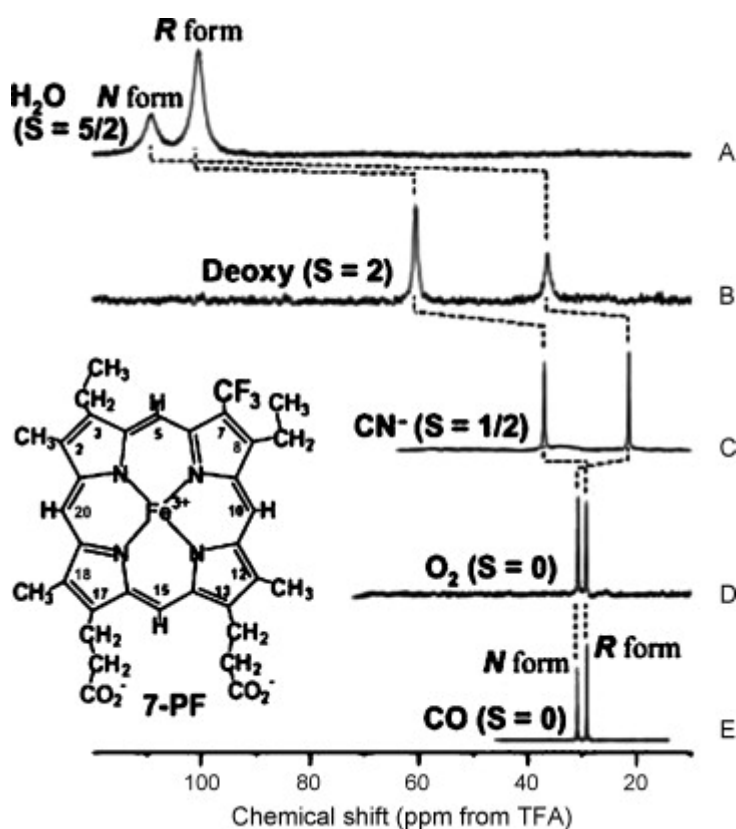
1. Download: Download full-size image

Fig. 1. (A–E) ^{19}F NMR spectra of various form of myoglobin substituted by the fluorinated heme 7-PF with various oxidation, spin (S) and ligation states of heme iron at pH 7.0 and 25 °C. The two well-separated signals reflected the fractions of the two isomers (N and R forms) due to the orientation disorder. From [26] with permission.

The two well-separated signals observed in each spectrum in Fig. 1 and the unequal intensities of the signal in the spectra reflected the fractions of the two isomers due to the two possible heme orientations [27]. The pair of heme orientations differ by a 180° rotation around the 5–15 H *meso*-proton axis (Fig. 1, N and R forms).

The heme iron is either in ferrous or ferric state with a number of electrons in the 3d orbitals of 6 and 5, respectively. Depending upon the spin pairing of electrons in the 3d orbitals, ferrous heme iron can have 4, 2 or 0 unpaired electrons, corresponding to $S = 2$, 1 or 0, respectively and for ferric heme iron $S = 5/2$, 3/2 or 1/2 with 5, 3 or 1 unpaired electrons, respectively. Based on an octahedral ligand field, the energy levels of the five 3d orbitals of the iron atom are split into two groups in such a way that the energies of the d_{z2} and d_{x2-y2} orbitals are higher than those of the other three orbitals d_{xy}, d_{yz} and d_{xz}. The spin state of the hemoproteins depends on the chemical nature of the ligand. The binding of a relatively weak field strength ligand such as H_2O on ferric heme iron gives a high-spin state $S = 5/2$ (Fig. 1A) and a low-spin state $S = 1/2$ is achieved with a ligand such as CN^- (Fig. 1C). For the ferrous heme iron, the deoxy form (Fig. 1B) is penta-coordinated with a high-spin configuration ($S = 2$) and the oxy form (Fig. 1D) or carbonmonoxy form (Fig. 1E) possesses a low-spin configuration ($S = 0$). Large variations occur between the ferric derivatives of both high- and low-spin state. Also indicative of the high sensitivity of the fluorine resonances are the variations observed for the ferrous states between the paramagnetic high-spin state (Fig. 1B) and the diamagnetic states (Fig. 1D and E). Only weak differences

are observed between the diamagnetic oxyform and carbonmonoxy complexes.

Paramagnetic ^{19}F NMR spectra of iron(III) porphyrins substituted with CF$_3$ groups and *met*myoglobin reconstituted with the iron complex of a 3-trifluoromethyl porphyrin have been measured and the ^{19}F shifts compared with the respective chemical shifts of the free ligands and zinc(II) complexes [25]. The shifts provided a diagnostic means for identifying the spin states.

Recently a deprotonation/protonation process in ferric myoglobin has been characterized by ^{19}F NMR [28] (pK_a determination, temperature dependence of the line width, …).

Computational methods have also been developed to predict the ^{19}F NMR chemical shifts in paramagnetic metalloporphyrins [29], [30].

3.2. ^{19}F NMR and fluorinated amino acids

Synthetic methods have been developed for preparation of fluorinated derivatives of numerous common amino acids and some of them are commercially available. Introduction of fluorine on amino acid could help to distinguish between different effects. An array of molecular biology protocols (site-directed mutagenesis, incorporation of modified amino acid, …) allows to explore the role of specific residue close to the metallic center especially from aromatic amino acids.

#### 3.2.1. Role of a targeted amino acid

The copper proteins with the type 1 active site (or blue proteins) are involved in electron transfer and are characterized by an intense blue color in the oxidized state arising from a ligand to metal charge transfer [31]. The involvement of the axial ligand on the reduction potential has been debated for a long time [32], [33], [34]. To probe the precise role of the axial methionine in azurin (Az), a well-known type 1 copper protein (Fig. 2(a)), a series of isostructural methionine replacements have been investigated including methyl fluorinated thioethers [35]. The replacement of the methionine ligand by isostructural unnatural amino analogues was performed using the express protein ligation method [36] that couples a bacterially expressed N-terminal protein to a synthetic C-terminal peptide containing the unnatural amino acids at the axial ligand position. This approach allows to probe one variance (geometry, steric or electronic interactions, solvent exposure, …) contrarily to multiple variances introduced by mutation.
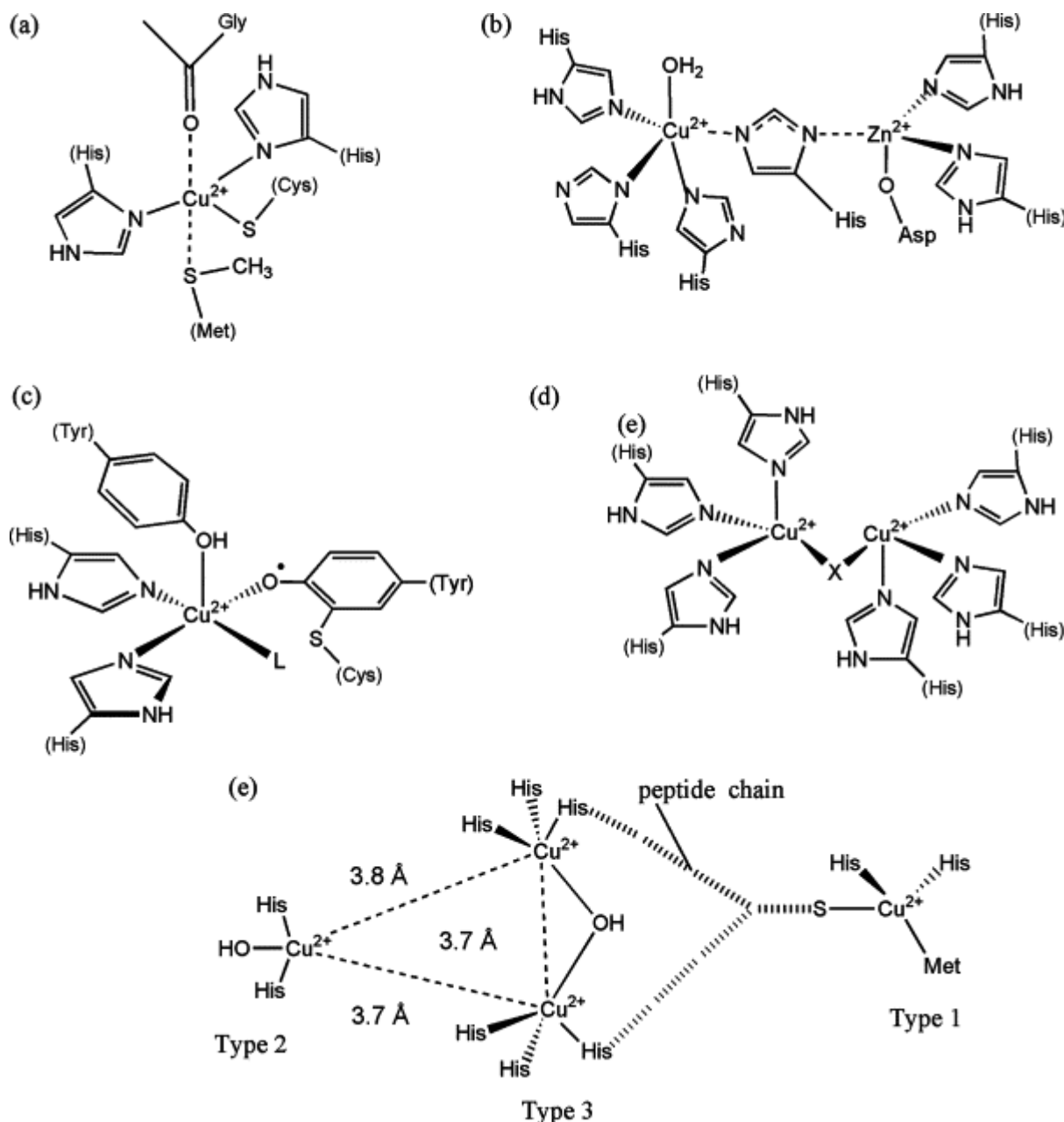
Fig. 2. Schematic representations of active sites of copper proteins presented herein: (a) azurin (type 1), (b) superoxide dismutase (type 2), (c) galactose oxidase (type 2), (d) X = OH or OH_2: catechol oxidase and tyrosinase (type 3), and (e) ascorbate oxidase (type 4 or multicopper oxidase).

As a result the correlation between reduction potentials and their axial ligand variants establishes hydrophobicity as the dominant factor in reduction potential tuning by the axial ligand. For fluorinated aminoacid the fluorine atoms are both adjacent to the methionine sulfur with the difluoro and trifluoro methionine entities (DFM and TFM, respectively, see Fig. 3). In contrast to the minor changes observed in the chemical shifts on azurin containing TFM (Az-TFM), the ^{19}F chemical shift on azurin containing DFM (Az-DFM) is significantly deshielded compared to reported DFM analogue in a nonparamagnetic environment. The former interacts more strongly with the copper ions than TFM although it is somewhat less sensitive to environmental factors than DFM. Interestingly, in Az-DFM the two fluorine atoms are diastereotopic; hence their chemical shifts are nonequivalent resulting in coupling between the two fluorine as well as proton coupling to each fluorine atom. Proton-decoupled ^{19}F spectrum displays two sets of broad doublets at 85.60 and 88.15 ppm. In freely rotating DFM only a broad signal should be observed. Herein the ^{19}F chemical shift nonequivalence in Az-DFM is enhanced, indicating a restricted conformational mobility of DFM in the protein. These observations point out to what extent the ^{19}F NMR chemical shifts are environment sensitive and can get new insights on environment factors.
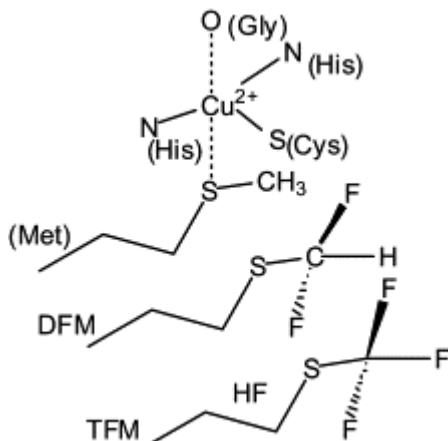
Fig. 3. Schematic representation of the blue copper center in Az showing replacement of the axial ligand methionine (Met) with fluorinated unnatural amino acids difluoromethionine (DFM) and trifluoromethionine (TFM). Redraw from Lu and co-workers [35].

3.2.2. Probe to study solvent exposure

When ^{19}F atom is solvent exposed, both chemical shift and T_1 relaxation are sensitive to interaction with the solvent. The T_1 relaxation time becomes longer and the ^{19}F resonance frequency shows an isotopic shift when the aqueous solvent is changed from H_2O to D_2O [37]. An interesting application is the use of the solvent-induced isotopic effect to estimate the degree of exposure of fluorine-containing proteins to the solvent. Illustrative example of ^{19}F NMR parameters used as a probe of solvent accessibility, is the work on a high-potential iron protein that contains a [Fe_4S_4] cluster from *Chromatium vinosum* [38], [39]. Fluorine-labeled protein were obtained by site-directed mutagenesis, or by inducing the expression of the protein in a medium supplemented with the fluorinated-derivative replacing a targeted amino acid (phenylalanine, tryptophan or tyrosine). ^{19}F combined with 2D ^{1}H/^{15}N NMR experiments indicate that solvent accessibility to the cluster is similar and minimal for the native proteins, but increases significantly for mutant proteins [38]. In addition fluorine NMR provides a probe of redox-dependent conformational changes [39]. Owing to the importance of determining solvent accessibility for the understanding of substrate binding chemistry and the control of the redox properties in metalloproteins, the strategies illustrated herein are of general interest and value.

3.3. Fluoride ion in presence of metalloproteins

3.3.1. Probe for exchangeable ligand on galactose oxidase

Galactose oxidase (GOase), a type 2 copper protein that catalyses the oxidation of primary alcohols into aldehydes [40].

Before the resolution of the X-ray structure, fluoride ion was used as a probe for the coordination site [41], [42]. The temperature and frequency dependence of the ^{19}F spin–spin R_2 and spin lattice R_1 relaxation rates of F$^-$ in the presence of the enzyme galactose oxidase have been analyzed. Evidence for a second coordination site for an exogenous ligand has been obtained from cyanide-fluoride competition studies, supported by ^{19}F NMR relaxation rate changes. The results are consistent with two exogenous binding sites, one equatorial with CN$^-$ and F$^-$ strongly binding the Cu^{II} center, and one axial with F$^-$ weakly bound. These results are in accordance with X-ray crystallographic data reported later [43]. The crystal structure reveals a mononuclear center with two nitrogen from histidine, two oxygen from tyrosine (one axial and one equatorial) and an additional equatorial exogenous ligand L (L = H_2O in the native enzyme). The active oxidized form possesses an equatorial bound tyrosyl radical (Fig. 2(c)).

3.3.2. Binding parameters of F$^-$ to metallic centers

The interaction of fluoride anion F$^-$ with a protein can be described according to the following equilibrium characterized by K (in M^{-1}) the stability constant.

$$(26) \quad E + F^- \rightleftharpoons E - F^-$$

The concentration C_{EF} of the paramagnetic complex E–F$^-$ is given by the following formula:

$$(27) \quad C_{EF} = \frac{KE_0 C_{F0}}{1 + KC_{F0}}$$

where E_0 is the concentration of the enzyme and C_{F0} is the concentration of the F$^-$ anion, in large excess on E_0.

The observed relaxation rate R_1 of the studied solution is the averaged mean by molar fractions for each species with the relaxation rate contributions of the anion in the bulk R_{10} and that of the anion in the complex $R_{1M} x_{EF}$ according to the following formula:

$$(28) \quad R_1 = R_{10} + R_{1M} x_{EF}$$

where $x_{EF} = C_{EF}/C_{F0}$ with $C_{EF} \ll C_{F0}$, *i.e.*

x_{EF} ■ 1. R_{10} and R_{1M} are the relaxation rates of the F$^-$ anion in the bulk, and bonded to the paramagnetic ion center within the protein, respectively. The paramagnetic contribution to the relaxation $R_{1p} = R_1 - R_{10}$ is therefore given using the following formula:

$$(29) \quad R_{1p} = \frac{R_{1M} K C_{E0}}{1 + K C_{F0}}$$

giving the two data, the stability constant K and the relaxation rate constant R_{1M} of the F$^-$ bonded to the paramagnetic site of the protein. Treatments of experimental data are usually reported from the R_{1p} plot as a function of log C_{F0} or T_{1p} as a function of C_{F0}.

3.3.2.1. Binding of F$^-$ to Cu/Zn superoxide dismutase

Superoxide dismutases (SOD) are redox heterobinuclear enzymes, which protect cells against superoxide ions toxicity [44]. Copper–zinc superoxide dismutase contains in its active site an imidazolate-bridged bimetallic center, with one copper(II) and one zinc(II) ion [45] depicted in Fig. 2(b). The Cu^{II} ion is coordinated by four histidine ligands in a distorted square planar coordination sphere, and by a fifth axial water ligand. The tetrahedral zinc ion is coordinated by three histidine ligands, one of them bridging to the copper and also by a carboxylate group. Fluoride anion binds at, or near the copper sites of the bovine or yeast superoxide dismutase, and the paramagnetic metals exert an enormous effect on the fluorine T_1 relaxation time in the bound state [46]. Contrarily to this large effect, the Cu/Zn SOD EPR spectra are only slightly affected by the presence of F$^-$ up to 3 M [47]. Details of the binding have been investigated in SOD by fluoride relaxation time determinations, in concert with water-proton relaxation studies, and by examining the paramagnetically shifted resonances of ligands near the metal centers [48]. The treatment of the experimental data gives the value 6 M^{-1} for the stability constant of the anion to SOD and the value of 1.5×10^6 s^{-1} for the spin-lattice relaxation rate of F$^-$ in the F$^-$-SOD complex. Furthermore, the increase of the water proton relaxation rate upon addition of F$^-$ suggest that, in this system, F$^-$ displaces the water ligand and binds it through an hydrogen bond.

An application of this large fluorine T_1 relaxation effect of such an enzyme has been used, in early stages of neuroimaging to quantify the presence of these enzymes in rat brain [49], [50].

3.3.2.2. F$^-$ to probe the accessibility of metallic centers in RNR and MMO

A set of experiments was done with two binuclear non-heme ferric center proteins: the small subunit of ribonucleotide reductase (RNR), protein R2 and the hydroxylase component of the soluble methane monooxygenase (MMO), protein A (Fig. 4) [51], [52]. They both catalyze oxygen activation and oxidations, but the substrates are different: for protein R2, the substrate is a specific tyrosine of the polypeptide chain in proximity to iron and for protein A, the substrates are different sized exogenous hydrocarbons, including methane. Although similarity can be found between the iron centers, there are different substrates involved, suggesting major differences between the two enzymes in terms of the accessibility of the metal ion sites. The F$^-$ anion has been used to study the electrostatic control for the accessibility of the metal ion center. Because Mn^{2+} is a much stronger relaxing agent than Fe^{3+}, the study was carried out with the manganese-containing forms of proteins R2 and A, prepared through the iron-free apoform [53].
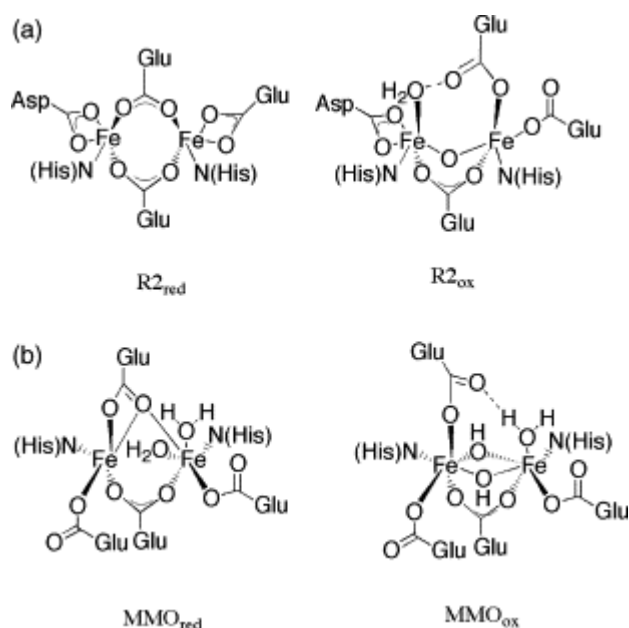
1. Download: Download full-size image

Fig. 4. Schematic representations of binuclear iron non-heme centers (reduced and oxidized state) in (a) R2 subunit in RNR and (b) hydroxylase component of soluble MMO.

For the Mn-A protein, treatment of the experimental data gives the value of 3 M^{-1} for the affinity constant of the anion to the protein and the value of 0.15×10^6 s^{-1} for the spin-lattice relaxation rate of F$^-$ in the F$^-$–Mn-A complex. For the protein Mn-R2, which contains four Mn^{2+} ions, no change of the relaxation rate of F$^-$ has been observed at any F$^-$ concentration. This demonstrates that the active site is buried in the protein and F$^-$ does not gain access to the metal ion site of ribonucleotide reductase.

These results emphasize that ^{19}F NMR combined to F$^-$ binding studies is a tool to access structural and dynamics of paramagnetic metallic centers. It is a useful complement to X-ray studies to further insights into solution in assessing dynamic properties.

3.4. Interactions of metalloproteins with fluorinated small molecules

3.4.1. Binding and reaction of fluorophenols on tyrosinase

Tyrosinases (Tyr) and catechol oxidases (CO) are essential type 3 (two Cu^{2+} in strong interaction) dicopper-containing enzymes. Tyrosinases occur in all living organisms, whereas catechol oxidases are found in plants. Tyrosinases mediate the hydroxylation of monophenols to o-diphenols as well as the subsequent

oxidation to quinones with dioxygen, whereas catechol oxidases catalyze the two-electron oxidation of o-diphenols to quinones (catecholase activity) (Fig. 2(d)). In fruit and vegetables Tyr and CO are key enzymes in the browning that occurs upon bruising or long-term storage. In mammals, Tyr are responsible for skin, eye and hair pigmentation. Both enzymes possess three identified forms of the active site in the catalytic cycle: *met* (Cu^{II}–Cu^{II}), *oxy* (Cu^{II}–O$_2^{2-}$–Cu^{II}) and *deoxy* (Cu^{I}Cu^I). The crystal structure of tyrosinase, has been obtained in 2006 from a recombinant enzyme [54] (the structure of *met* and *deoxy* forms of catechol oxidase were previously obtained [55]). In the *met* form all six histidine residues are conserved among Tyr and CO and exhibit a very similar binding geometry (Fig. 2(d)). The two copper(II) ions, are bridged by an aquo or an hydroxo entity.

The activity of Tyr from *Streptomyces antibioticus* toward the three isomeric fluorophenols (o-FP, m-FP, p-FP) was studied in detail and evidenced different behavior in solution (Fig. 5) [56]. The reaction of m-FP and p-FP in the presence of Tyr produced polymeric species. When the enzymatic reactions of m-FP and p-FP were carried out in presence of a reductant (ascorbic acid), formation of polymeric species was completely quenched. In both cases, ^{19}F NMR spectra show the peak of the starting phenol and a resonance at −126.7 ppm (Fig. 5) assigned to the same catechol derivative.
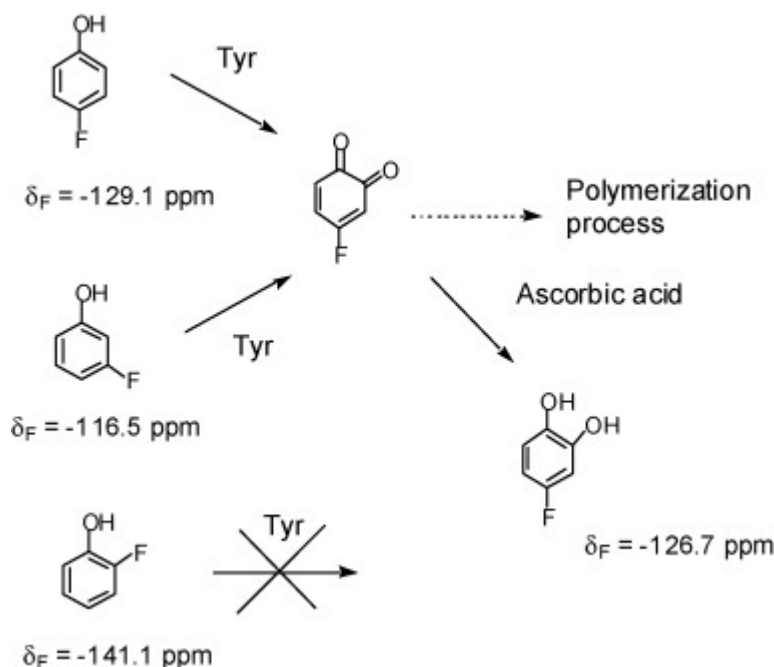
1. Download: Download full-size image

Fig. 5. Products formed in the early steps of the reaction of o-, m- and p-FP and Tyr. Fluorine chemical shifts are reported relative to CFCl$_3$. From Casella and co-workers [56].

Incubation of the mixture with o-FP shows the lack of reactivity with or without ascorbic acid: o-FP acts as a competitive inhibitor in the enzymatic oxidation of l-Dopa, the natural substrate of Tyr. In this work the ^{19}F NMR appears as a complementary technique to the more conventional kinetic and optical spectroscopic methods. The binding studies with fluorinated phenol lead to reliable information on reaction intermediates and get new insights in mechanistic comprehension.
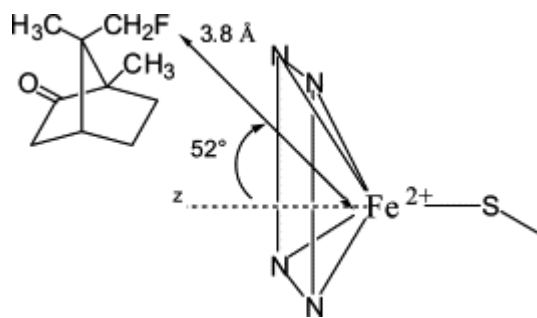
3.4.2. Inhibitor binding studies on ascorbate oxidase

The copper site in ascorbate oxidase (AO) is composed of four copper atoms involved in the four-electron reduction of dioxygen to water, with concomitant one-electron oxidation of the reducing organic substrate [57] (Fig. 2(e)). A type 2 and a type 3 active site together form a trinuclear cluster. An additional type 1 site is connected through a Cys-His electron transfer pathway to the trinuclear cluster at a distance of 12 Å (Fig. 2(e)). The binding mode of the former phenolic substrates on ascorbate oxidase have been studied by Casella and co-workers [58] to provide experimental support of the location of the inhibitor binding site. Paramagnetic ^{19}F NMR relaxation measurements have been performed on AO in presence of o-FP or p-FP (m-FP after addition on the protein causes protein precipitation). Relaxation rate R_{1obs} was measured for the fluorine atom of the inhibitor at different enzyme concentrations, in order to obtain information about the distance of fluorine from copper ions contained in the active site of AO. From the value of R_{1obs}, R_{1b} (for the bound inhibitor when this is in fast exchange between the active site and the bulk solution) has been calculated from the equation: $(30) R1obs–R1f=(R1b–R1f)E0KI+I0$ where R_{1f} is R_1 for the free inhibitor, E_0 and I_0 are the initial enzyme and inhibitor concentrations, respectively, and K_I (unit M) is the dissociation constant for the enzyme–inhibitor complex. The paramagnetic contribution to the relaxation rate R_{1M} of the fluorine nucleus of the bound inhibitor arising from the unpaired electron on the copper center(s), is related to the copper–fluorine distance by the Solomon–Bloembergen–Morgan equation (Eqs. (8), (9), Section 2.2). As the inhibitor is not bound to the metal center, only the dipolar term has been retained in the former equation.

The ^{19}F relaxation data agree with a binding site of the bound o- or p-FP inhibitors close to the type 1 copper center while the contribution to relaxation of the bound inhibitors by the type 2 Cu site is negligible (Fig. 2(e)). An estimation of the Cu–F distances for the protein complexes with o- and p-FP from the $1/T_{1b}$ values is 5.4 and 5.9 Å, respectively. Information obtained from this study is of general interest indicating that for both inhibitors and substrates of AO, the binding site is located in a pocket near the type 1 copper center.

3.4.3. Spatial interaction from heme and fluorinated substrate

Considering a similar approach, spatial interaction relationships between a heme and its substrate have been determined [59]. Relaxation and chemical shifts data were analyzed (in absence of strong hyperfine interactions) affording an estimation of the distance between the heme iron of ferrous cytochrome P-450 and a fluorine substrate analogue (9-fluorocamphor) (Fig. 6). Furthermore the chemical shifts data analysis gives the orientation of 9-fluorocamphor within the normal heme and the Fe■F vector heme (Eq. (22)). The former angle and the Fe■F distance estimated, are nearly comparable with those observed by X-ray crystallography of the ferric camphor-bound enzyme.

Fig. 6. Schematic representation of the ferrous high-spin heme iron of P-450 and 9-fluorocamphor bound in the active site based on [59].

These studies clearly demonstrate that tightly bound fluorinated substrate analogues can be successfully used to determine metal to substrate (or inhibitor) distances and geometrical information within the paramagnetic active site.

4. Applications to paramagnetic metal complexes of biological interest

4.1. Paramagnetic complexes in solution

^{19}F NMR has sometimes been used with bioinspired fluorinated mimics (*vide infra*). It has also been used to study solution equilibria. A not exactly new but typical example is the study in acetone solution of the conformational equilibria in pyridine adducts of metal (cobalt, nickel) hexafluoroacetylacetonates [60]. Complexes 1:1 and 1:2 (two pyridines) were observed. In the case of the cobalt complexes, both *cis*- and *trans*-isomers were detected. At room temperature the various isomers are in rapid equilibrium and the ^{19}F NMR lines are averaged. At lower temperature, the rate of exchange is slowed down, and well-resolved NMR spectra are observed for all the possible isomers. The NMR shift of the signal from the nickel complex is mainly due to the Fermi contact interaction, while the shifts of lines from the various cobalt complexes are due to both the electron–fluorine dipolar interaction, and the Fermi contact interaction.

^{19}F NMR has been used to investigate intramolecular effects of copper(II) ions on the fluorine chemical shifts of dioxane complexes of copper perfluorocarboxylates [61].

In a more recent work, a ^{19}F longitudinal specific relaxation rate or relaxivity (r_1, s^{-1} M^{-1}) study of the competition of Gd^{III} and Lu^{III} towards diethylenetriaminepentacetate (DTPA) in water is described [62]. The Gd^{III} aqua ion and Gd-DTPA cause very different longitudinal relaxivities of the trifluoroacetate anion ^{19}F nuclei. In the presence of competitor Lu^{III} ions, the relaxivity difference makes it possible to assay the concentrations of Gd^{III} aqua ions and Gd-DTPA complex from the measured paramagnetic relaxation rate enhanced by of the trifluoroacetate ^{19}F nuclei.

A variety of cobalt(II/III) and iron(II/III) complexes have been prepared containing the ligands 4-fluoro-2,2′bipyridine (fbpy) and anion hexafluorophosphate [63]. Both *fac*- and *mer*-isomers of [M(fbpy)$_3$]$^{m+}$ have been described. ^{19}F NMR chemical shifts allow the determination of the ratio of each isomer. The ^{19}F chemical shifts of the ligand show minor variations with changes in the anion or solvent, while a larger variation is found as a function of the oxidation state of the metal (~7 ppm for the change from Co^{III} to Co^{II} and ~38 ppm for the change from Fe^{III} to Fe^{II}). Moreover, variable temperature ^{19}F NMR allows a mechanistic study of electron transfer in Co^{II}(bpy)$_3$$^{2+}$–Co^{III}(fbpy)$_3$$^{3+}$ system.

4.2. Biomimetic models

4.2.1. Fluorinated porphyrins

Many proteins contain a removable heme that can be easily replaced by a fluorinated fragment (see above). Taking advantages of this technique, extensive studies have been performed on synthetic porphyrins labeled by fluorine, a CF$_3$ or a fluorinated aromatic group.

As ^{19}F NMR has been extensively studied on a series of halogenated porphyrins, the former have been employed to interpret the ^{19}F chemical shifts of paramagnetic compounds. A special library with different types of fluorine splitting patterns for tetrakis(pentafluorophenyl) porphyrins (TFPP) (Fig. 7) complexed with diamagnetic (Zn) and paramagnetic (Cu, Fe, Ru) metal ions [64] has been created (Table 1).
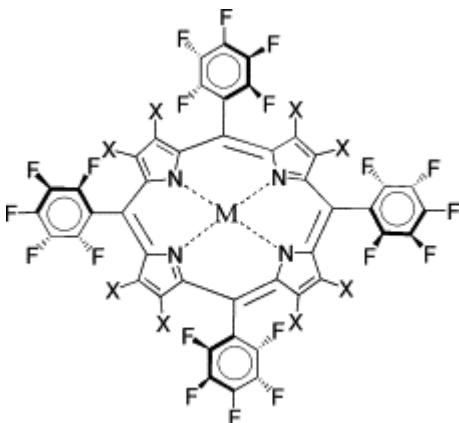
Fig. 7. Schematic representations of tetrakis(pentafluorophenyl) porphyrins (TFPP) series with M = H$_2$, Zn, Cu, Fe, Ru and X = H, Cl, Br. Redraw from [64].

Table 1. NMR shift for a series of fluorinated porphyrins (TFPP) from [64]

Compound	Ortho	Para	Meta
^{19}F shifts NMR value in acetone-d_6 [a]			
ZnTFPP	−138.5 (d)	−154.8 (t)	−163.7 (m)
H$_2$TFPP	−136.9 (d)	−151.7 (t)	−161.8 (m)
FeTFPP(Cl)	−105.8, −107.7	−150.2	−153.9, −156.0
FeTFPP(OH)	−108.0, −114.5	−152.0	−156.6, −158.0
(FeTFPP)$_2$O	−133.3, −137.1	−154.8	−163.1, −164.7
CuTFPP	Not observable [b]		
ZnTFPPCl$_8$	−138.9 (d)	−151.5 (t)	−163.4 (m)
H$_2$TFPPCl$_8$	−140.0 (d)	−149.8 (t)	−162.4 (m)
RuTFPPCl$_8$(CO) [c]	−138.8, −139.3	−151.3 (t)	−163.2, −163.6
RuTFPPCl$_8$(py)$_2$	−136.9 (d)	−149.7 (t)	−161.1 (m)
ZnTFPPBr$_8$	−138.4 (d)	−151.7 (t)	−163.1 (m)
H$_2$TFPPBr$_8$	−139.7 (d)	−150.1 (t)	−162.7 (m)
FeTFPPBr$_8$(Cl)	−121.4, −122.3	−146.5	−158.1, −158.5
[FeTFPPBr$_8$(Cl)]$^-$	−124, −133	−148	−158, −160
FeTFPPBr$_8$(py)$_2$ [d]	−138.6	−152.0 (t)	−163.1 (m)

a

^{19}F NMR values are vs. CFCl$_3$ at 0 ppm. Fine structure given as follows: d, doublet of doublets; t, triplet; m, multiplet.

b

Cu(II) species are not generally observable due to their long relaxation time.

c

Major set of resonances, each with fine structure as observed in diamagnetic species; other resonances also observed, as discussed in text.

d

Values in CDCl$_3$.

The paramagnetic shift, line broadening and fine structure of resonances from the peripheral pentafluorophenyl rings are, dependent on the symmetry and core environment of the porphyrins macrocycles, as evidenced on value collected in Table 1.

The chemical shifts of the fluorine atoms on the *meso*-phenyl rings are extremely sensitive to the metal center, to its axial ligands, and to the pyrrole carbon substituents. However, each porphyrin will have a unique spectrum. The ^{19}F NMR spectra for the unmetalated and zinc TFPP and TFPPBr$_8$ complexes (Table 1), display one set of signals each with fine structure for the *o*-, *m*-, and *p*-F.

Substitution with a paramagnetic or an axially asymmetric metal center, results in significantly different NMR spectra. High-spin, five-coordinate Fe^{III}TFPP(Cl) and FeTFPP(OH) samples show five separate ^{19}F NMR signals that fall over a much larger window than those of the diamagnetic porphyrins. The five-coordinate (FeTFPP)$_2$O dimer shows five peaks in its NMR spectrum (Table 1); however, the signals show significantly less broadening and appear in a much narrower window than those of the other Fe^{III} porphyrins. Strong antiferromagnetic coupling, between the two metal centers reduces the paramagnetic shift in the ^{19}F NMR of the *p*-oxo dimer. The distinctive patterns observed in ^{19}F NMR play important roles in the structural assignment of other perhalogenated compounds. The ^{19}F NMR spectrum of Fe^{III}TFPPBr$_8$(Cl) shows a broadened five-signal pattern similar to that of FeTFPP(Cl). The *o*-F resonances exhibit a smaller paramagnetic shift in the perhalogenated compound. The addition of pyridine to Fe^{III}TFPPBr$_8$(Cl) results in reduction of the iron, and formation of the symmetric bis(pyridine) compound Fe^{II}TFPPBr$_8$(py)$_2$. The identification of this compound was confirmed as low-spin iron(II) due to the sharp signals and splitting pattern consistent with an axially symmetric, diamagnetic species. Most unusual is the NMR of [Fe^{II}TFPPBr$_8$(Cl)]$^-$, produced by electrochemical reduction of Fe^{III}TFPPBr$_8$(Cl). The relatively sharp signals support the reduction of the metal center, but the splitting of the *o*- and *m*-signals suggests an axially asymmetric porphyrin; the Fe^{II} porphyrin appears to retain an association with the chloride ligand even in the reduced state.

Another series with pentafluorophenyl-substituted iron(III) porphyrinates, has also been investigated and compared with the respective protonated phenyl-substituted iron porphyrinates [65]. The fluorinated phenyl compounds all show large *o*-F isotropic shifts while the *m*-F and *p*-F isotropic shifts are much smaller in magnitude, but have the same sign as the *o*-F isotropic shifts of each complex, even when there is significant spin density at the *meso*-carbons. Unlike the ^{1}H isotropic shifts, which are readily separable into dipolar and contact contributions, the ^{19}F isotropic shifts of the *o*-fluorines have an overriding large contribution from either a ligand-centered dipolar shift, or a through-space contact shift that results from direct electron cloud overlap of the *o*-fluorines with the π system of the porphyrin ring, but in either case, the large isotropic shift of the *o*-fluorines appears to be related to the spin density at the *meso*-carbon to which the fluorinated phenyl group is attached. Difluorovinyl deuteroporphyrin iron complexes have been synthesized and it has been shown that the ^{19}F chemical shifts were also very sensitive to the spin state of the metal and the nature of the ligand [24].

Fluorine NMR has also been used to investigate the dioxygen-reactivity of iron(II) heme [66] and heme–copper complexes [67]. Such studies provide insights on the O$_2$ binding process, on the new types of dioxygen adducts and on decomposition process.

4.2.2. Fluorinated models of non-heme diiron enzymes

Carboxylate-bridged diiron centers (Fig. 4) are encountered at the active sites of enzymes that bind or activate dioxygen (hemerythrin, methane monooxygenase, ribonucleotide reductase, Δ^9-desaturase, …) [51], [52], and diverse synthetic models of their active sites have been synthesized and studied [68], [69]. ^{19}F NMR has been used to investigate the carboxylate coordination on diiron(II) model complexes and its shifts [70], [71]. In a very nice paper, Lippard and co-workers [72]

provided compelling evidence for dynamic core rearrangements via fluoro-substituted carboxylate shifts, using variable temperature ^{19}F NMR from di(carboxylato) to tetra(carboxylato) diiron(II) complexes (Fig. 8).
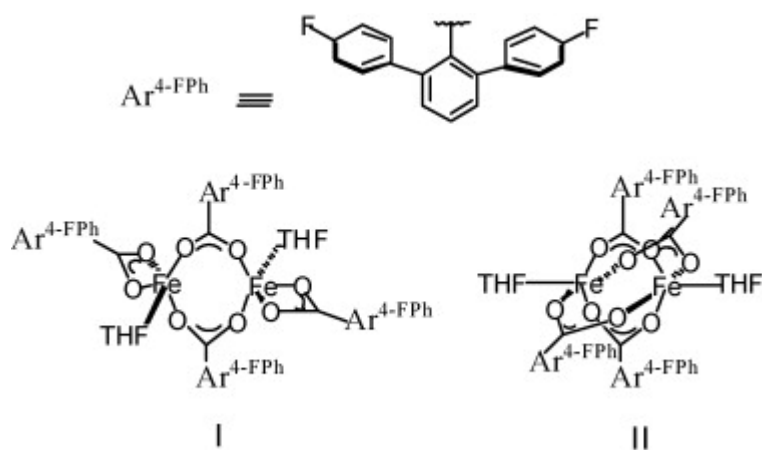
1. Download: Download full-size image

Fig. 8. Redraw after Lippard and co-workers [72].

The dramatic spectral change of the doubly bridged diiron(II) complex I from +20 to −80 °C (Fig. 9) is interpreted as an equilibration between doubly bridged (I) and quadruply bridged isomers (II) (Fig. 8). Temperature dependent core interconversions evidenced from ^{19}F NMR, could facilitate attack by an incoming dioxygen molecule at an open coordination site for binding and activation during catalysis.
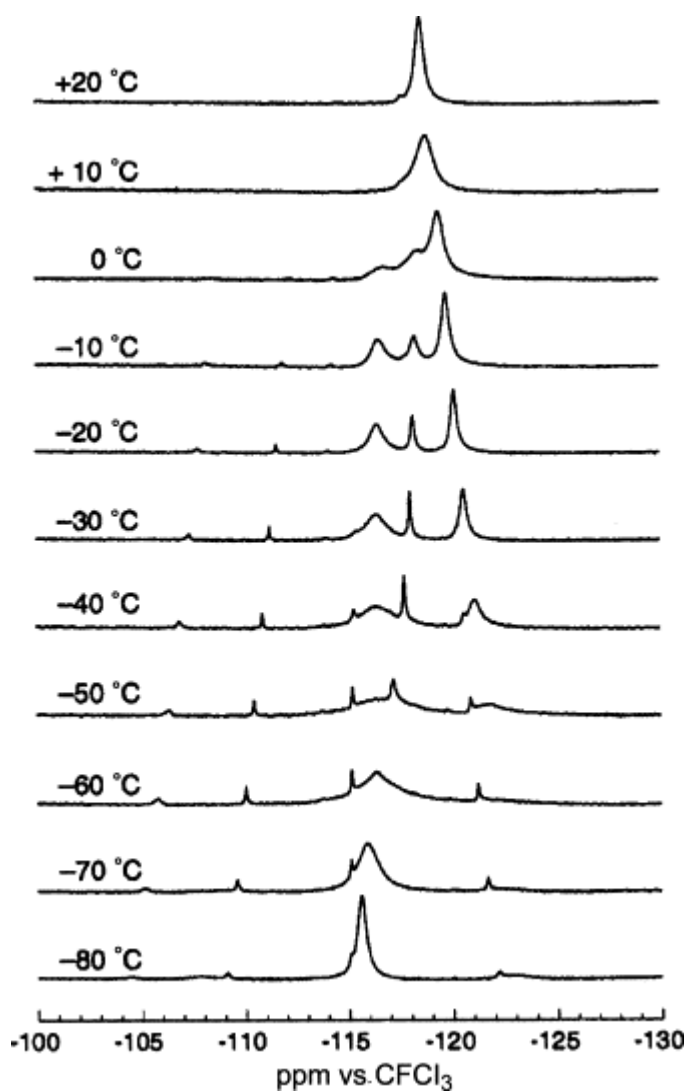
1. Download: Download full-size image

Fig. 9. Variable-temperature ^{19}F NMR spectra (vs. CFCl$_3$) of compound I in CH$_2$Cl$_2$. From [72] with permission.

4.2.3. Fluorinated models of galactose oxidase

From copper(II) complexes of tripodal ligand HLq^{NO2} (Fig. 10), depending on the experimental conditions (varying the respective amount of Cu^{2+}) complexes **1** and **1H** (Fig. 10) have been isolated and characterized (X-ray) [73]. The protonation state of the phenol moiety and its position (axial vs. equatorial) were probed

by ^{19}F NMR in relation with galactose oxidase enzyme (Fig. 2(c)). The fluorine NMR behavior for each species, present different chemical shifts (δ_F = 49.0 and 53.7 ppm), and different line width at half intensity of the resonance ($\nu_{1/2}$ = 25 and 250 Hz) for **1** and **1H**, respectively. These data clearly evidence the different environment of the copper(II) center viewed from a fluorine nucleus inserted in the ligand. In addition, from an equimolar mixture of **1** and **1H**, dynamic data were obtained through the collapse of **1** and **1H** species in chemical exchange. At the temperature of coalescence of the two signals (T_c = 226 K), the rate constant of the exchange k = 3000 ± 100 s^{-1} is determined according to Eq. (31) [74], indicating that molecular rearrangement (proton transfer and isomerization) between **1** and **1H** is fast:

$$k = \pi \Delta \nu \sqrt{2} \quad (31)$$
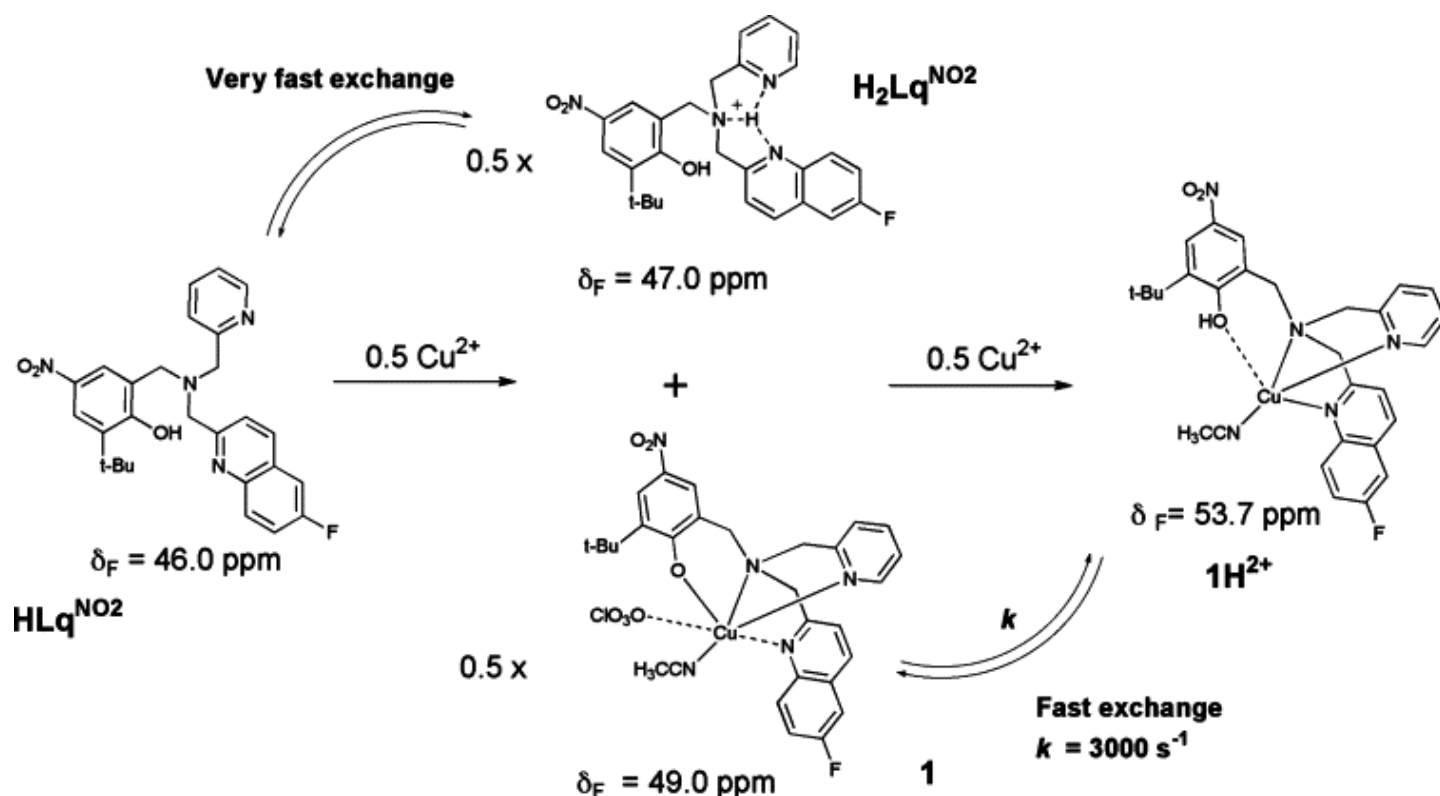
1. Download: Download full-size image

Fig. 10. Reaction of HLq^{NO2} with Cu^{2+} (0–1 equiv. added) ^{19}F NMR studies done at 282.4 MHz.

4.2.4. Fluorine-labeled catechol oxidase models

4.2.4.1. [19]F to monitor pH-dependent equilibrium

From ligand HL$_F$, a fluorinated model (Fig. 11) as been studied which is either bis aqua, μ-hydroxo bridged or bis hydroxo according pH (the two first species have been characterized from X-ray structure determination) [75]. [19]F chemical shift are given in Table 2.
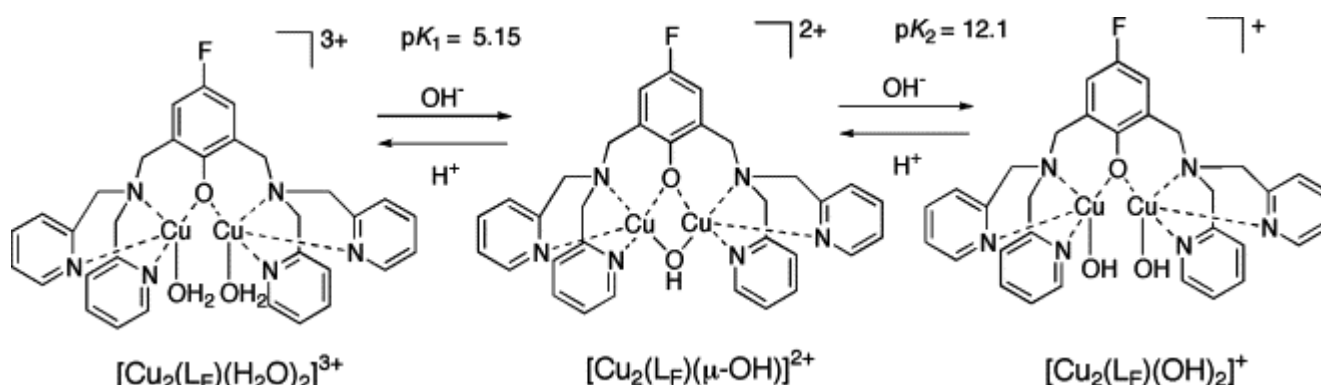
1. Download: Download full-size image

Fig. 11. pH-driven interconversions between dinuclear complexes from ligand HL$_F$.

Table 2. [19]F chemical shifts (ppm vs. C$_6$F$_6$) of [Cu$_2$(L$_F$)(μ-OH)]$^{2+}$ and [Cu$_2$(L$_F$)(H$_2$O)$_2$]$^{3+}$ complexes in D$_2$O/DMSO (8/2, v/v)

Compound	δ_F
HL$_F$	32.0
[Cu$^{II}_2$(L$_F$)(H$_2$O)$_2$]$^{3+}$	65.5
[Cu$^{II}_2$(L$_F$)(μOH)]$^{2+}$	43.3
[Cu$^{II}_2$(L$_F$)(OH)$_2$]$^{+}$	51.5
[Cu^{II}Cu^{I}(L$_F$)(OH)]$^{+}$	22.7

The mixed valence complex $[Cu^{II}Cu^{I}(L_F)(\mu OH)]^+$ has also been obtained. The ^{19}F NMR spectra of the EPR silent μOH complex exhibits a relatively sharp peak, compared to the spectra of the bis aqua complex which presents a broad resonance peak. Despite that the fluorine atom is far from the metal centers, ^{19}F chemical shifts are drastically dependent on the changes in the metal coordination spheres. Moreover, ^{19}F chemical shifts are an efficient probe of the redox states of the metal centers: a $\Delta\delta$ of 20.6 ppm is observed between the μ-hydroxo dicopper(II) complex from HL_F and the one-electron reduced corresponding complex. The pH-driven interconversions have also been monitored by ^{19}F NMR. The spectra are depicted in Fig. 12. Starting from $[Cu_2(L_F)(\mu OH)]^{2+}$ spectrum, characterized by a single resonance at 43.3 ppm, addition of increasing amount of $HClO_4$ in the solution leads to the appearance of a new signal which is clearly observed at 65.5 ppm. The new signal grows at the expanse of the original resonance. In acid medium, only the new signal remains and it corresponds to the resonance found for the isolated $[Cu_2(L_F)(H_2O)_2]^{3+}$ (Table 2). The same behavior can be observed, when an increasing amount of NaOH is added to the $[Cu_2(L_F)(\mu OH)]^{2+}$ solution. The direct mixing of HL_F, $Cu(ClO_4)_2$ and NaOH leads to the same complex (putatively $[Cu_2(L_F)(OH)_2]^+$) that the addition of NaOH to the characterized complex $[Cu_2(L_F)(\mu OH)]^{2+}$. ^{19}F NMR is proved to be a powerful tool to study quantitatively the pH-dependent equilibrium between the various complexes. The equilibrium processes are slow at the ^{19}F NMR time-scale, allowing the observation of the species simultaneously present in the medium. It has to be emphasized that, in the same conditions, the exchange is fast with regard to the ^1H NMR time-scale in relation with small chemical shift differences between the concerned chemical species.
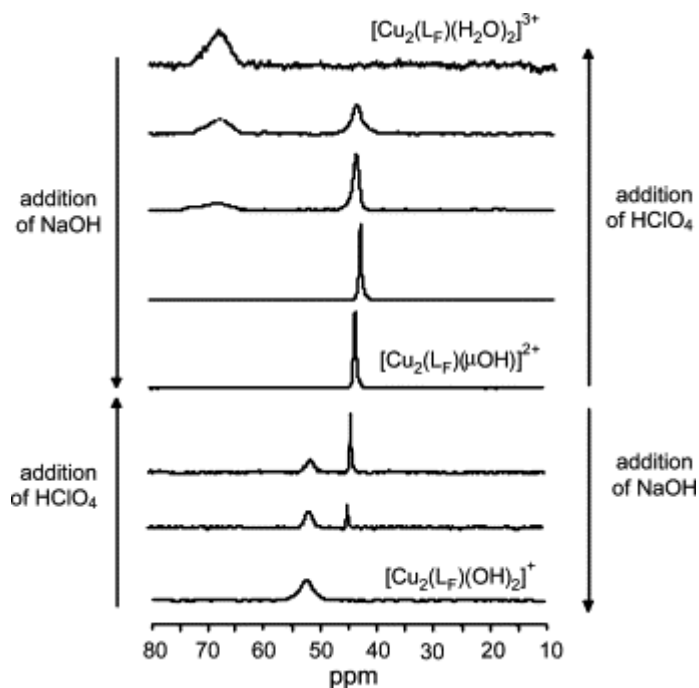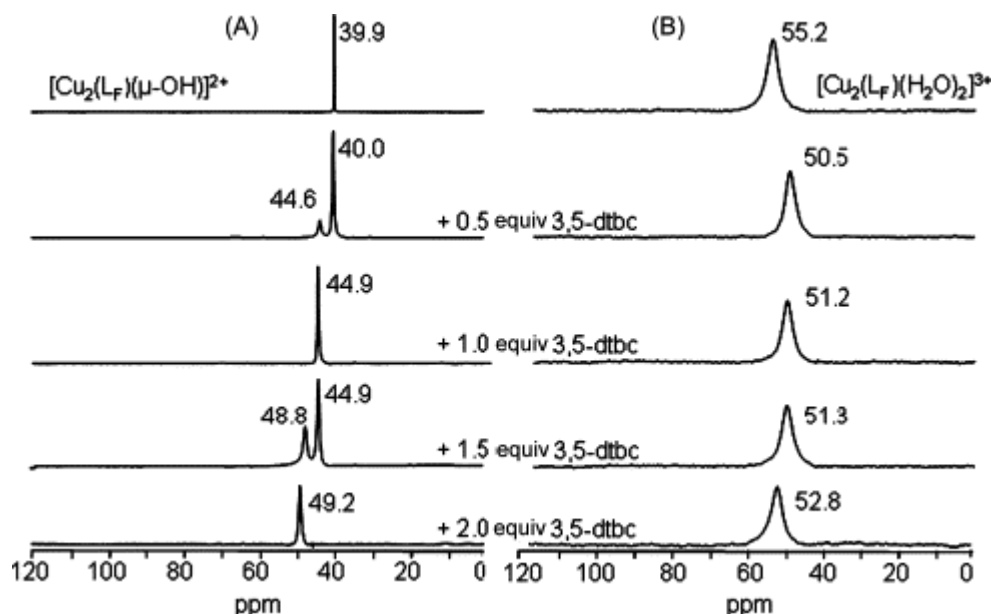

1. Download: Download full-size image

Fig. 12. ^{19}F NMR monitored titration of $[Cu_2(L_F)(H_2O)_2]^{3+}$ by NaOH in D_2O/DMSO (8/2, v/v). The same spectrum is obtained by addition of $HClO_4$ to $[Cu_2(L_F)(\mu OH)]^{2+}$. ^{19}F NMR spectra vs. C_6F_6.

4.2.4.2. Substrate binding studies

Modifications in the coordination sphere around bridged dicopper(II) centers are easily evidenced by changes in fluorine chemical shifts on ^{19}F NMR spectra. In Fig. 13 is depicted the evolution of the ^{19}F NMR spectra of the $[Cu_2(L_F)(\mu-OH)]^{2+}$ and $[Cu_2(L_F)(H_2O)_2]^{3+}$ complexes, respectively, upon progressive addition of 3,5-dtbc (3,5-di-*tert*-butylcatechol, a model substrate) in $[D_6]$acetone and in anaerobic conditions [76]. For $[Cu_2(L_F)(\mu-OH)]^{2+}$ (Fig. 13(A)), the resulting spectra exhibit well-resolved resonances. The equilibrium processes are slow compared to the ^{19}F NMR time-scale, allowing the observation of a mixture of two species simultaneously present in the medium. Spectra in Fig. 13 show that two products are successively formed upon addition of substrate (one and two molar equivalents), characterized by chemical shifts at 44.9 and 49.2 ppm, respectively. The ^{19}F NMR chemical shifts observed for each species are slightly modified due the presence of other compounds in solution. With the bis aqua complex $[Cu_2(L_F)(H_2O)_2]^{3+}$, a different behavior is observed (Fig. 13(B)). From the relatively broad signal of the starting material, the addition of one, then two molar equivalents of 3,5-dtbc leads to the formation of two different adducts characterized by signals located at 51.2 and 52.8 ppm, respectively. In the presence of 0.5 and 1.5 molar equivalents, the peaks broadening could also be due to exchange processes faster than the ^{19}F NMR time-scale in addition to the paramagnetic properties of the isolated species.
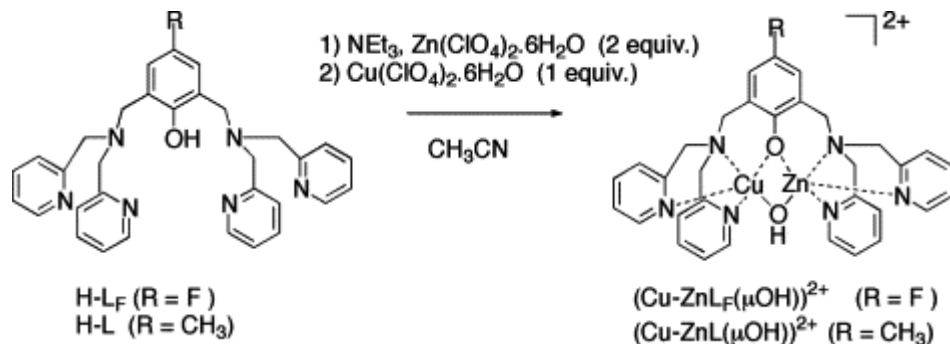
1. Download: Download full-size image

Fig. 13. ^{19}F NMR (ppm vs. C_6F_6) in [D_6]acetone for (A) [$Cu_2(L_F)(\mu\text{-OH})]^{2+}$ and (B) [$Cu_2(L_F)(H_2O)_2]^{3+}$; upon progressive addition of 3,5-dtbc (from 0 to 2 equiv.).

These observations underline the interest of ^{19}F NMR as a probe in mechanistic studies to complete UV–vis and EPR investigations. In the same conditions, the exchange is fast in regard to the ^1H NMR time-scale. Both [$Cu_2(L_F)(\mu\text{-OH})]^{2+}$ and [$Cu_2(L_F)(H_2O)_2]^{3+}$ species can bind one or two substrates, but *different adducts* are formed. From the hydroxo bridged species, the substrate binding occurs in two *successive* steps while on the contrary, from bis aqua complex, no successive steps can be clearly evidenced. Different binding processes of 3,5-dtbc have been evidenced herein.

### 4.2.5. Synthesis control of heterodinuclear complexes (a Cu^{II}–Zn^{II} example)

Although some non-heme proteins containing heterodinuclear metal centers are known (Fe–Zn purple acid phosphatase, Fe–Zn calcineurin, Zn–Mg in DNA polymerase I, Cu–Zn superoxide dismutase, *etc.*), only a limited number of synthetic models have been published, probably due to the difficulty of the syntheses. To prepare only the heterodinuclear complex from a dinucleating ligand, an experimental approach based on the ligand HL_F (Fig. 14) averred to be of particular interest to prepare the Cu–Zn complex described in Fig. 14 [77]. Furthermore, it can be directly applied in the NMR tube to test rapidly different experimental conditions to prepare the Cu–Zn complex (depicted in Fig. 14).

1. Download: Download full-size image

Fig. 14. Schematic preparation and structure of the (μ-phenoxo)(μ-hydroxo)Cu^{II}–Zn^{II} complexes.

Different experimental conditions were tested, upon varying the respective amount and concentration of HL_F, $Zn(ClO_4)_2 \cdot 6H_2O$ and $Cu(ClO_4)_2 \cdot 6H_2O$. Reactions are performed in acetonitrile solution with triethylamine (2 equiv.), in a NMR tube, and monitored directly by ^{19}F NMR. In Fig. 15 are depicted the spectra corresponding to the more significant experimental pathways. Mixing HL_F, $Zn(ClO_4)_2 \cdot 6H_2O$ with $Cu(ClO_4)_2 \cdot 6H_2O$ at 1:1:1 ratio (statistical method) leads to a mixture of different complexes. ^{19}F NMR spectroscopy exhibits three well-resolved resonances (Fig. 15(a)). Comparison with the δ_F of the homodinuclear (μ-phenoxo)(μ-hydroxo) (Cu^{II}–Cu^{II} or Zn^{II}–Zn^{II}) complexes isolated after an independent preparation, allowed the unambiguous identification of the bis copper (40.0 ppm) and the bis zinc (29.7 ppm) resonances, despite the small deviation of ^{19}F NMR chemical shift observed between these isolated complexes (40.7 and 30.4 ppm, respectively) and those in the reaction mixture. When using an excess of the zinc salt (HL_F, $Zn(ClO_4)_2 \cdot 6H_2O$, $Cu(ClO_4)_2 \cdot 6H_2O$ at 1:2:1 ratio) the dicopper complex is not observed, but still leads to a mixture (Fig. 15(b)). Interestingly, by using this last procedure, in a 2-fold diluted medium, and a later addition of the copper salt, only the compound with the signal at 31.9 ppm is obtained (Fig. 15(c)) and it can easily be isolated and characterized as the [Cu–$ZnL_F(\mu OH)$]($ClO_4)_2$. The ^{19}F NMR spectrum of this copper–zinc complex exhibits a relatively broad resonance compared to the spectra of the diamagnetic bis zinc complex and to the paramagnetic bis copper(II) complex (with no EPR observed spectrum), indicating a strong antiferromagnetic interaction between the two copper atoms as in the dibridged dinuclear copper(II) complex from HL [78]. EPR data for the heterobinuclear complex reveals the usual features of a mononuclear copper(II) complex with axial symmetry. These observations, taken together, indicate that the observed ^{19}F signals are very sensitive to the local environment (structural and magnetic) of this dimetallic center.
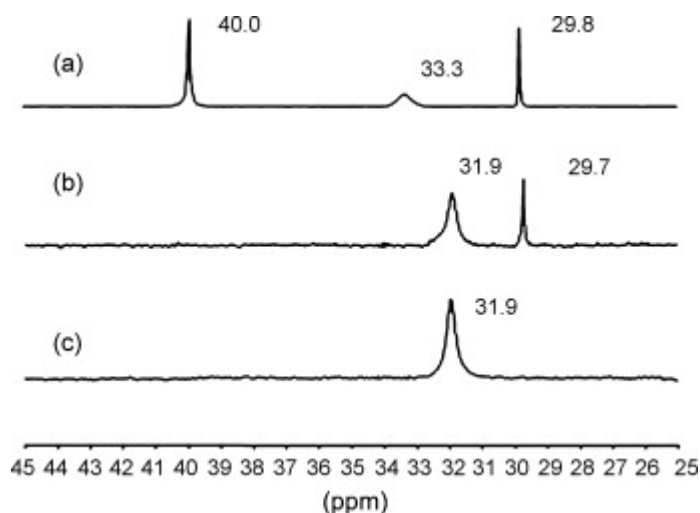
1. Download: Download full-size image

Fig. 15. ^{19}F NMR for (a) HL_F + 2Et$_3$N + 1Zn(ClO$_4$)$_2$·6H$_2$O + 1Cu(ClO$_4$)$_2$·6H$_2$O (10^{-3} M in CD$_3$CN); (b) HL_F + 2Et$_3$N + 2Zn(ClO$_4$)$_2$·6H$_2$O + 1Cu(ClO$_4$)$_2$·6H$_2$O (10^{-3} M in CD$_3$CN); (c) HL_F + 2Et$_3$N + 2Zn(ClO$_4$)$_2$·6H$_2$O + 1Cu(ClO$_4$)$_2$·6H$_2$O (10^{-5} M in CD$_3$CN). ^{19}F NMR spectra vs. C$_6$F$_6$.

Then, the same experimental procedure was applied with HL and enabled us to prepare and isolate easily the corresponding heterodinuclear [Cu–ZnL(μOH)](ClO$_4$)$_2$ complex, in good yield.

The current statistic process used to prepare heterobinuclear complexes leads to mixtures of homo and heterobinuclear species and no rapid method is available to analyze these mixtures before separation of the complexes. ^{19}F NMR can be a viable tool for adjusting experimental procedure in order to prepare, under control and good yield, heterodinuclear complexes.

5. Conclusion

Some conclusions emerge from these successful investigations of paramagnetic centers presented in this review.

The problem of spectral overlap encountered in ^1H NMR is removed in ^{19}F NMR. Simplification on the spectra, the easiness of (bio)synthetic incorporation and the low-perturbing nature of fluorine substitution (in size and electronic density especially at aromatic positions) emphasizes the benefit of this approach. ^{19}F chemical shifts as well as relaxation times lead to complementary and accurate information. The examples given in this review show that ^{19}F NMR can be efficiently used to study: (i) exchange equilibria according pH between different species, (ii) equilibria between stereoisomers, (iii) binding and spatial interactions of substrates to paramagnetic metal centers, (iv) redox and spin states of the metallic centers, (v) solvent exposure of active metallic center, and (vi) evidence of reaction intermediates.

Despite this, it is surprisingly underused. ^{19}F NMR is proved to be a powerful tool for structural as well as mechanistic (catalytic) studies for paramagnetic metal complexes and metalloenzymes.

Acknowledgement

References

[1]
J.T. Gerig
Methods Enzymol., 117 (1989), p. 3
View PDFView article
[2]
J.T. Gerig
Prog. Nucl. Magn. Reson., 26 (1994), p. 293
and references herein
View PDFView articleView in Scopus
[3]
B.D. Sykes, W.E. Hull
Methods Enzymol., 49 (1978), p. 270
View PDFView articleView in Scopus
[4]
Presentation of NMR data for publication in Chemical Journals: B—conventions relating to spectra from nuclei other than protons, Pure Appl. Chem., 1976, p. 217.
Google Scholar
[5]

G.N. La Mar, W.D. Horrocks, R.H. Holm (Eds.), NMR of Paramagnetic Molecules: Principles and Applications, Academic Press, New York (1973)

[6]

I. Bertini, C. Luchinat

Coord. Chem. Rev., 150 (Special issue) (1996), p. 1

View in Scopus

[7]

I. Bertini, C. Luchinat, G. Parigi (Eds.), Solution NMR of Paramagnetic Molecules, Elsevier, Amsterdam (2001)

[8]

I. Solomon

Phys. Rev., 99 (1955), p. 559

View in Scopus

[9]

I. Solomon, N. Bloembergen

J. Chem. Phys., 25 (1956), p. 261

View at publisherCrossref

[10]

R.E. Connick, D. Fiat

J. Chem. Phys., 44 (1966), p. 4103

View at publisherCrossrefView in Scopus

[11]

J. Reuben, G.H. Reed, M. Cohn

J. Chem. Phys., 52 (1970), p. 1617

View in Scopus

[12]

N. Benetis, J. Kowalewski, L. Nordenskiöld, H. Wennerström, P.O. Westlund

Mol. Phys., 48 (1983), p. 329

View at publisherCrossrefView in Scopus

[13]

J. Kowalewski

D.M. Grant, R.K. Harris (Eds.), Encyclopedia of Nuclear Magnetic Resonance, vol. T5, J. Wiley (1996), p. 3456

[14]

P.H. Fries

Mol. Phys., 48 (1983), p. 503

View at publisherCrossrefView in Scopus

[15]

E. Belorizky, P.H. Fries, L. Helm, J. Kowalewski, D. Kruk, R.R. Sharp, P.O. Westlund

J. Chem. Phys. (2008), p. 052315

View in Scopus

[16]

P.H. Fries, E. Belorizky

J. Chem. Phys., 126 (2007), p. 204503

View in Scopus

[17]

D. Canet, J.C. Boubel, E. Canet-Soulas

Wiley (Ed.), Nuclear Magnetic Resonance: Concepts and Methods, Chichester, New York (1996)

Google Scholar

[18]

B. Bleaney

J. Magn. Res., 8 (1972), p. 91

View PDFView articleView in Scopus

[19]

J.A. Peters, J. Huskens, D.J. Raber

Prog. Nucl. Magn. Reson., 28 (1996), p. 283

View PDFView articleView in Scopus

[20]

G.N. La Mar, G.R. Eaton, R.H. Holm, F.A. Walker

J. Am. Chem. Soc., 95 (1973), p. 63

View at publisher

CrossrefView in Scopus

[21]

L. Di Bari, P. Salvadori

Coord. Chem. Rev., 249 (2005), p. 2854

View PDFView articleView in Scopus

[22]

P. Fries, G.N. Patey

J. Chem. Phys., 80 (1984), p. 6253

[23]

M. Jeannin, E. Belorizky, P. Fries, W. Gorecki

J. Phys. II, 3 (1993), p. 1511

[24]

C. Poliart, J.-F. Briand, F. Tortevoie, J. Leroy, G. Simonneaux, A. Bondon

Magn. Reson. Chem., 39 (2001), p. 615

View in Scopus

[25]

H. Toi, M. Homma, A. Suzuki, H. Ogoshi

J. Chem. Soc., Chem. Commun. (1985), p. 1791

View in Scopus

[26]

A. Yamamoto

Annu. Rep. NMR Spectrosc., 57 (2006), p. 52

and references herein

[27]

G.N. La Mar, D.L. Budd, D.B. Viscio, K.M. Smith, K.C. Langry

Proc. Natl. Acad. Sci. U.S.A., 75 (1978), p. 5755

View at publisherCrossrefView in Scopus

[28]

S. Nagao, Y. Hirai, A. Suzuki, A. Yamamoto

J. Am. Chem. Soc., 127 (2005), p. 4146

View at publisher

CrossrefView in Scopus

[29]

J.G. Pearson, B. Montez, H. Le, E. Oldfield, E.Y.T. Chien, S.G. Sligar

Biochemistry, 36 (1997), p. 3590

View in Scopus

[30]

J. Mao, Y. Zhang, E. Oldfield

J. Am. Chem. Soc., 124 (2002), p. 13911

View in Scopus

[31]

E.I. Solomon, M.J. Baldwin, M.D. Lowery

Chem. Rev., 92 (1992), p. 521

View at publisher

CrossrefView in Scopus

[32]

B.G. Malmström, P. Wittung-Stafshede

Coord. Chem. Rev., 185–186 (1999), p. 127

View PDFView articleView in Scopus

[33]

H.B. Gray, B.G. Malmström, R.J.P. Williams

J. Biol. Inorg. Chem., 5 (2000), p. 551

View in Scopus

[34]

E.I. Solomon, R.K. Szilagyi, S. DeBeer George, L. Basumallick

Chem. Rev., 104 (2004), p. 419

View in Scopus

[35]

D.K. Garner, M.D. Vaughan, H.J. Hwang, M.G. Savelieff, S.M. Berry, J.F. Honek, Y. Lu

J. Am. Chem. Soc., 128 (2006), p. 15608

View at publisher

CrossrefView in Scopus

[36]

K. Severinov, T.W. Muir

J. Biol. Chem., 273 (1998), p. 16205

View PDFView articleView in Scopus

[37]

P.E. Hansen, H.D. Dettman, B.D. Sykes

J. Magn. Res., 62 (1985), p. 487

View PDFView articleView in Scopus

[38]

D. Li, A. Agarwal, J.A. Cowan

Inorg. Chem., 35 (1996), p. 1121

View in Scopus

[39]

D. Li, A. Soriano, J.A. Cowan

Inorg. Chem., 35 (1996), p. 1980

View in Scopus

[40]

J.W. Whittaker

A.S.H. Sigel (Ed.), Metal Ions in Biological Systems, Marcel Dekker, New York (1994), p. 315

Google Scholar

[41]

R.J. Kurland, B.J. Marwedel

J. Phys. Chem., 83 (1979), p. 1422

View at publisher

CrossrefView in Scopus

[42]

B.J. Marwedel, D.J. Kosman, R.D. Bereman, R.J. Kurland

J. Am. Chem. Soc., 103 (1981), p. 2842

View at publisher

CrossrefView in Scopus

[43]

N. Ito, N.E.V. Phillips, K.D.S. Yadav, P.F. Knowles

J. Mol. Biol., 238 (1994), p. 794

View PDFView article

[44]

I. Fridovich

Annu. Rev. Biochem., 11 (1975), p. 147

View at publisherCrossrefView in Scopus

[45]

J.A. Tainer, E.D. Getzoff, J.S. Richardson, D.C. Richardson

Nature, 306 (1983), p. 284

View at publisher

CrossrefView in Scopus

[46]

P. Viglino, A. Rigo, R. Stevanato, G.A. Ranieri, G. Rotilio, L. Calabrese

J. Magn. Res., 34 (1979), p. 265

View PDFView articleView in Scopus

[47]

I. Bertini, E. Borghi, C. Luchinat, A. Scozzafava

J. Am. Chem. Soc., 103 (1981), p. 7779

View at publisher

CrossrefView in Scopus

[48]

L. Banci, I. Bertini, C. Luchinat, A. Scozzafava, P. Turano

Inorg. Chem., 28 (1989), p. 2377

View at publisher

Crossref

[49]

M. Scarpa, P. Viglino, F. Momo, F. Bracco, L. Battistin, A. Rigo

J. Biochem. Biophys. Methods, 22 (1991), p. 135

View PDFView articleView in Scopus

[50]

M. Scarpa, F. Vianello, A. Rigo, P. Viglino, F. Bracco, L. Battistin

Magn. Reson. Chem., 11 (1994), p. 697

[51]

A.L. Feig, S.J. Lippard

Chem. Rev., 94 (1994), p. 759

View at publisher

CrossrefView in Scopus

[52]

L.J. Que, Y. Dong

Acc. Chem. Res., 29 (1996), p. 190

View in Scopus

[53]

S. Hamman, M. Atta, A. Ehrenberg, P. Wilkins, H. Dalton, C. Béguin, M. Fontecave

Biochem. Biophys. Res. Commun., 195 (1993), p. 594

View PDFView articleView in Scopus

[54]

Y. Matoba, T. Kumagai, A. Yamamoto, H. Yoshitsu, M. Sugiyama

J. Biol. Chem., 281 (2006), p. 8981

View PDFView articleView in Scopus

[55]

T. Klabunde, C. Eicken, J.C. Sacchettini, B. Krebs

Nat. Struct. Biol., 5 (1998), p. 1084

View in Scopus

[56]

G. Battaini, E. Monzani, L. Casella, E. Lonardi, A.W.J.W. Tepper, G.W. Canters, L. Bubacco

J. Biol. Chem., 277 (2002), p. 44606

View PDFView articleView in Scopus

[57]

A. Messerschmidt

K.D. Karlin, Z. Tyeklar (Eds.), Bioinorganic Chemistry of Copper, Chapman & Hall, New York (1993), p. 471

View at publisher

CrossrefGoogle Scholar

[58]

L. Santagostini, M. Gullotti, L. De Gioia, P. Fantucci, E. Franzini, A. Marchesini, E. Monzani, L. Casella

Int. J. Biochem. Cell Biol., 36 (2004), p. 881

View PDFView articleView in Scopus

[59]

G.B. Crull, J.W. Kennington, A.R. Garber, P.D. Ellis, J.H. Dawson

J. Biol. Chem., 264 (1989), p. 2649

View PDFView articleView in Scopus

[60]

P.F. Richardson, R.W. Kreilick

Inorg. Chem., 20 (1981), p. 1978

View at publisher

CrossrefView in Scopus

[61]

A.V. Sobolev, S.A. Krupoder, T.I. Liskovskaya, V.S. Danilovich

J. Struct. Chem., 41 (2000), p. 338

View in Scopus

[62]

C.S. Bonnet, P. Fries

Magn. Reson. Chem., 41 (2003), p. 782

View at publisher

CrossrefView in Scopus

[63]

F. Qu, T.Q. Nguyen, A.F. Janzen

J. Fluorine Chem., 94 (1999), p. 15

View PDFView articleView in Scopus

[64]

E.R. Birnbaum, J.A. Hodge, M.W. Grinstaff, W.P. Shaefer, L. Henling, J.A. Labinger, J.E. Bercaw, H.B. Gray

Inorg. Chem., 34 (1995), p. 3625

View at publisher

CrossrefView in Scopus

[65]

L. Yatsunyk, F.A. Walker

Inorg. Chim. Acta, 337 (2002), p. 266

View PDFView articleView in Scopus

[66]

R.A. Ghiladi, R.M. Kretzer, I. Guzei, A.L. Rheingold, Y.-M. Neuhold, K.R. Hatwell, A.D. Zuberbühler, K.D. Karlin

Inorg. Chem., 40 (2001), p. 5754

View in Scopus

[67]

R.A. Ghiladi, E.E. Chufan, D. del Rio, E.I. Solomon, C. Krebs, B.H. Huynh, H.-W. Huang, P. Moënne-Loccoz, S. Kaderli, M. Honecker, A.D. Zuberbühler, L. Marzilli, R.J. Cotter, K.D. Karlin

Inorg. Chem., 46 (2007), p. 3889

CrossrefView in Scopus

[68]

J. Du Bois, T.J. Mizoguchi, S.J. Lippard

Coord. Chem. Rev., 200–202 (2000), p. 443

View PDFView articleView in Scopus

[69]

E.V. Tshuva, S.J. Lippard

Chem. Rev., 104 (2004), p. 987

View in Scopus

[70]

K.S. Hagen, R. Lachicotte, A. Kitaygorodskiy

J. Am. Chem. Soc., 115 (1993), p. 12617

CrossrefView in Scopus

[71]

R. Lachicotte, A. Kitaygorodskiy, K.S. Hagen

J. Am. Chem. Soc., 115 (1993), p. 8883

CrossrefView in Scopus

[72]

D. Lee, S.J. Lippard

Inorg. Chem., 41 (2002), p. 2704

View in Scopus

[73]

F. Michel, S. Hamman, F. Thomas, C. Philouze, I. Gautier-Luneau, J.L. Pierre

Chem. Commun. (2006), p. 4122

CrossrefView in Scopus

[74]

J.A. Pople, W.G. Schneider, H.J. Bernstein

High-Resolution Nuclear Magnetic Resonance

McGraw-Hill, New York (1959)

p. 223

Google Scholar

[75]

C. Belle, C. Béguin, I. Gautier-Luneau, S. Hamman, C. Philouze, J.L. Pierre, F. Thomas, S. Torelli, E. Saint Aman, M. Bonin

Inorg. Chem., 41 (2002), p. 479

View in Scopus

[76]

S. Torelli, C. Belle, S. Hamman, J.L. Pierre, E. Saint Aman

Inorg. Chem., 41 (2002), p. 3983

View in Scopus

[77]

S. Torelli, C. Belle, I. Gautier-Luneau, S. Hamman, J.L. Pierre

Inorg. Chim. Acta, 333 (2002), p. 144

View PDFView articleView in Scopus

[78]

S. Torelli, C. Belle, I. Gautier-Luneau, J.L. Pierre, E. Saint Aman, J.M. Latour, L. Le Pape, D. Luneau

Inorg. Chem., 39 (2000), p. 3526

View in Scopus

Cited by (18)

Charge density distribution effect in pyrrolidine-fused chlorins on microbial uptake and antimicrobial photoinactivation of microbial pathogens

2021, Journal of Photochemistry and Photobiology B: Biology

Citation Excerpt :

This structural feature produces an increment of the amphiphilic character, which can be advantageous for the uptake of microbial cells. Moreover, PFP groups can also be used for 19F magnetic resonance imaging in combination with red fluorescence imaging of the chlorin macrocycle for biomedical investigations [40–42]. In addition, fluorinated porphyrinoids usually have higher photostability towards oxidative degradation than the corresponding unsubstituted fluorine analogs [15].

Show abstract

New frontiers and developing applications in ^{19}F NMR

2013, Progress in Nuclear Magnetic Resonance Spectroscopy

Citation Excerpt :

Indeed, this has been used to identify cellular compartmentation based on the ability of the contrast agent to relax extracellular, but not intracellular material [159]. Direct relaxation can also be achieved by including F or CF3 in a paramagnetic ligand complex [113,160]. If 19F is attached very close to a paramagnetic center, such as Gd3+ or Fe3+, the local paramagnetic relaxation effect (PRE) can strongly influence the fluorine atom.

Fluorinated porphyrinoids and their biomedical applications

2011, Journal of Photochemistry and Photobiology C: Photochemistry Reviews

Citation Excerpt :

Thus, 19F NMR detects the fluorine containing molecule selectively and reduces the problem with background signals. Moreover, this technique is more sensitive for changes in the microenvironment than 1H NMR due to larger chemical shifts [34–36]. 19F NMR can be used for in vitro investigation of molecules containing fluorine, e.g. their interaction mechanisms with receptors, anticancer drug localization in tumors and normal tissues.

Show abstract

New porphyrins tailored as biodiesel fluorescent markers

2011, Dyes and Pigments

Citation Excerpt :

The resulting equations extracted from the curves were used to quantify markers 2 and 3 in the biodiesel samples. The synthesis of the novel tetra-functionalized (pentafluorophenyl)porphyrins 2 and 3 was accomplished by means of the highly selective nucleophilic substitution of the four para-fluoro atoms in the 5,10,15,20-meso-tetrakis-(pentafluorophenyl)porphyrin (1) using an improvement to a described procedure [17]. The products were obtained in high yields (98 and 95%, respectively) by using hexadecan-1-ol, in THF, or ethanol as nucleophiles under reflux, as shown in Scheme 1.

Show abstract

NMR spectroscopic investigations of transition metal complexes in organometallic and bioinorganic chemistry

2024, Bulletin of the Korean Chemical Society

Applications of Fluorous Porphyrinoids: An Update[†]

2021, Photochemistry and Photobiology

View all citing articles on Scopus

View Abstract

Recommended articles

Accurate fragment-based 51-V chemical shift predictions in molecular crystals

Solid State Nuclear Magnetic Resonance, Volume 114, 2021, Article 101733

Amanda Mathews, Joshua D. Hartman

View PDF

Refining the anchor: Optimizing the performance of cyclometallated ruthenium(II) dyes in p-type dye sensitized solar cells

Polyhedron, Volume 140, 2018, pp. 122-128

Nathalie Marinakis, …, Catherine E. Housecroft

View PDF

Long-lived negative molecular ions of TCNQ formed by the resonant capture of electrons with above zero energies

Chemical Physics Letters, Volume 711, 2018, pp. 81-86

Olga G. Khvostenko, …, Svetlana N. Tseplina

View PDF

Show 3 more articles

Article Metrics

Citations

- Citation Indexes: 18

Captures

- Readers: 42

- About ScienceDirect
- Remote access
- Shopping cart
- Advertise
- Contact and support
- Terms and conditions
- Privacy policy

Cookies are used by this site. Cookie settings | Your Privacy Choices